Contrib Mineral Petrol (2001) 140: 701–719
DOI 10.1007/s004100000215

E. A. Dunworth · E.-R. Neumann · J. M. Rosenbaum

The Skien lavas, Oslo Rift: petrological disequilibrium and geochemical evolution

Received: 30 September 1999 / Accepted: 12 October 2000 / Published online: 12 January 2001

Abstract The Skien lavas, which form the earliest phase of basaltic magmatism within the Permo-Carboniferous Oslo Rift, contain multiple generations of clinopyroxene which exhibit strong petrological and geochemical disequilibrium. Three principal core compositions have been identified: (1) low-jadeite, high-Mg, Cr-diopside cores (CrMgDi) with strongly depleted trace-element signatures, which are believed to be xenocrystic in origin; (2) Mg-rich, Cr-poor diopside cores (MgDi) with moderately depleted trace-element signatures which probably represent early cognate growth; and (3) more dominant, low-Mg, phenocrystic diopside cores (PhenDi). Several samples contain CrMgDi or MgDi cores which have been subjected to resorption and partial re-equilibration with their host melts, indicative of extensive disequilibrium and magma mixing. These three core types are overgrown by trace-element-enriched Ti-augite, which also forms megacrysts and late-stage lava groundmass. Calculated Ti-augite/melt partition coefficients show clinopyroxene compatibility of the M-HREE, Zr, Hf and Y. The LILE, Sr, and Nb remain incompatible. ϵSr_{300} and ϵNd_{300} of Ti-augite overgrowths, phenocrystic diopside, and MgDi diopside cores show that intrasample isotopic disequilibrium existed when the host basalts were erupted. All epsilon values lie within the range of data previously published for the Skien lavas. Detailed examination of the chemical, isotopic and textural disequilibrium features seen in these lavas has enabled us to place constraints upon the magmatic evolution of this basalt suite, ranging from xenocryst incorporation to cognate multistage pyroxene growth, as well as identifying clear evidence of magma mixing and possible crustal contamination.

E. A. Dunworth (✉)
Mineralogisk-Geologisk Museum,
Sars'gate 1, 0562 Oslo, Norway
E-mail: lizzyann@magma.ca

E.-R. Neumann
Department of Geology,
Universitetet i Oslo, Postboks 1047 Blindern,
0316 Oslo, Norway

J. M. Rosenbaum
PRIS, University of Reading,
P.O. Box 227 Whiteknights, Reading,
Berks, UK

J. M. Rosenbaum
Present address: Geochemical Solutions Ltd.,
31 Harpsden Road, Henley-on-Thames,
Oxon RG9 1EE, UK

Editorial responsibility: I. Parsons

Introduction

Most geochemical studies of igneous rocks have assumed, often out of analytical necessity, that the samples being studied were formed under equilibrium conditions. Whereas petrographic descriptions have sometimes shown evidence of disequilibrium crystallization (e.g., Duda and Schmincke 1985; Dunworth and Wilson 1998; Neumann et al. 1999), it has often been difficult to assess the degree of corresponding geochemical and isotopic disequilibrium preserved within individual samples, particularly between individual mineral phases, or even between different generations of growth of a single phase. Such combined petrographic and geochemical characterizations are important for three primary reasons: (1) to fully understand the relevance (and limitations) of "whole-rock" analyses (i.e., isochrons, trace-element data, calculated initial isotopic ratios, etc.); (2) to identify the mantle (and crustal) sources that have contributed to the magmas; and (3) to characterize the magmatic evolution of the rocks being studied.

The Skien "basalts" (alkali basalts, tephrites and nephelinites), which erupted in the earliest stages of Permo-Carboniferous B1 basaltic magmatism within the Oslo Rift (Sundvoll et al. 1990), offer an excellent opportunity for the study of disequilibrium crystallization since samples taken from many of the flows in the ~1,500-m-thick sequence are clearly not in petrographic or geochemical equilibrium. Our aim was to characterize

the type and degree of petrographic and geochemical disequilbrium within the Skien basalts, focussing in particular on the disequilibrium features exhibited by the multiple types of clinopyroxene found within the volcanic sequence, and to examine the problems associated with integrating these features into a model of magmatic evolution. It should be noted that, in the context of this study, the term "dissolution" is defined as the combination of chemical reaction or resorption (kinetics) and partial melting (thermodynamics) that occurs when a crystal encounters a melt with which it is not in thermodynamic equilibrium.

Previous work

The Permo-Carboniferous Oslo Rift, along with its associated magmatic events, has been the subject of many petrogenetic (Segalstad 1979; Neumann 1986; Schou-Jensen and Neumann 1988; Neumann 1994), geochemical (Anthony et al. 1989; Neumann et al. 1988, 1990), structural (Sundvoll and Larsen 1994; Heeremans et al. 1996) and geophysical studies (Ramberg 1976; Ro et al. 1990).

The NNE-SSW-trending rift contains three major sections: the northern Akershus segment, the central Vestfold segment, and the southern (submarine) Skaggerak graben. Five stages of rifting, lasting from about 315 to 240 Ma, are described in Ramberg and Larsen (1978). The earliest basaltic activity began ~300 Ma ago on the southwestern flank of the Vestfold segment, with the eruption of ~1,500 m of nephelinitic-basaltic flows at Skien (Fig. 1), and it is this sequence of flows which is the focus of the present study. Earlier petrogenetic and geochemical studies of the Skien basalts by Segalstad (1979), Neumann et al. (1988) and Anthony et al. (1989) have already shown preliminary evidence of multiple generation of clinopyroxene growth, intrasample Sr-Nd isotopic disequilibrium, and the fact that at least one of the mantle sources tapped by the Skien lavas was not involved in the genesis of any of the other basaltic sequences found within the Oslo Rift.

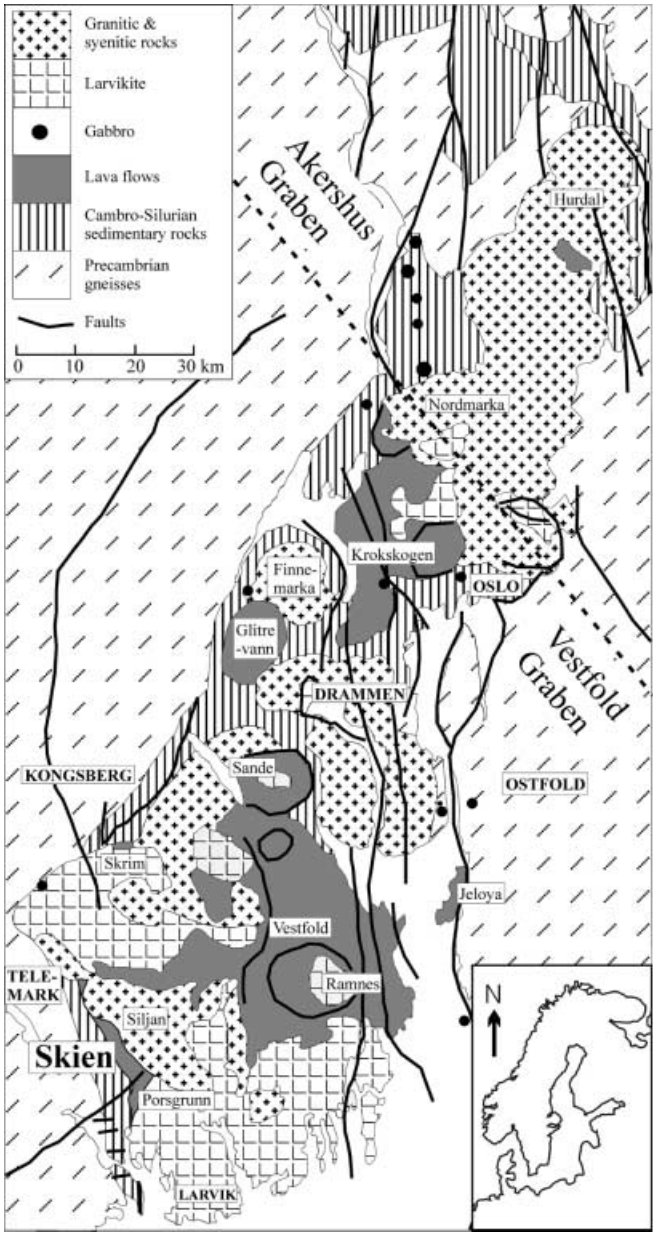

Fig. 1 Map of the onshore section of the Oslo Rift (after Ramberg and Larsen 1978). The Skien basalts represent the most south-western basaltic activity within the rift. The main sampling site is located just NE of the "n" of Skien, while the Porsgrunn road-cut is located just north of the main fault cutting through the southern part of the Skien basalt area

Analytical methods

Major-element analyses of pyroxenes were carried out with a Caméca Camebax microprobe at the Geologisk Museum, Oslo, using a 15-kV, 20-nA beam, and 10 s counting times for all elements except Cr and Ni (30 s). Analyses were calibrated using silicate standards: albite or omphacite (Na), K-feldspar (K), wollastonite (Ca, Si), and oxides (Al, Mg, Fe, Mn, Ti, Cr, Ni). Duplicate analyses using forsterite (Mg) and fayalite (Fe) standard calibrations produced similar results within the limits of analytical precision. Data reduction was carried out using PAP Caméca software. Analytical precision is estimated to be better than ±1% for oxides >20 wt%, ±2% for oxides in the range 10–20 wt%, ±5% for oxides in the range 2–10 wt%, and <10% for elements in the range 0.3–2 wt% (Neumann et al. 1999; this study).

Trace-element abundances of the pyroxenes were determined at the University of Edinburgh Ion Microprobe Facility with a modified Caméca IMS 4f ion microprobe using a ~15–20-μm-diameter, ~5-nA O^- primary beam. In order to reduce molecular interference, only positive secondary ions with initial energies of 55–95 eV were analyzed. Peak-stripping corrections were made for molecular interferences of BaO, BaAl, BaSi, rare earth element (REE) oxides, and REEs-Al and REEs-Si where

necessary. On the basis of the repeated testing of primary and internal secondary silicate and pyroxene standards with a similar matrix composition, all other molecular interferences were assumed to be negligible. Accuracy for all elements is ±3–10% except for Hf (±16%; 1σ error). Element intensity ratios were measured relative to Si whose content was verified by electron microprobe (accuracy ±1%). Element contents were calculated on the basis of ion yields from NIST SRM 610 silicate glass analyzed under the same conditions (Hinton et al. 1995) and normalised to the NIST SRM 610 "preferred average" trace-element contents of Pearce et al. (1997). While we realise that the latter values are based on ICPMS rather than ion-probe determinations, the Pearce et al. (1997) values have been used to ensure internal consistency with a LAM-ICPMS data set obtained from related samples from the Oslo Rift which will be published separately and which has been normalised using the NIST SRM 610 and 612 values of Pearce et al. (1997).

For geochemical whole-rock and pyroxene mineral-separate analyses, the samples were first split using a hydraulic splitter and jaw crusher. The gravels were subsequently ground to a fine powder (<10 μm) in a steel shatterbox for whole-rock geochemical analysis, or fed through a sieve crusher from which pyroxene separates (500–250 μm) were obtained by magnetic separation and handpicking.

Major-element whole-rock analyses were obtained by XRF (Universitetet i Oslo) and trace-element analyses by ICP-MS (Actlabs, Ontario). Analytical precision for the former is given by Neumann et al. (1990), and for the latter by Dunworth and Bell (2001).

Sr-Nd isotopic analyses were carried out at the Geologisk Musuem, Oslo using a VG Micromass 54 (Rb, Sr, Sm) and a Finegan-MAT 262 (Nd) mass spectrometer. Pyroxene separates were ground to ~10 μm in alcohol with a corundum pestle and mortar. Both the pyroxene and whole-rock powders were washed in ethanol and water and subsequently leached in 6N HCl at 100 °C for 4 h before being dried, weighed, and dissolved. Dissolution was carried out in sealed 15-ml Savillex beakers using a HNO_3-HF mixture held at 120 °C for 48 h. Subsequent chemical and mass spectrometric procedures were based on those described by Mearns (1986) and Neumann et al. (1990).

It should be noted that the sample numbering schemes of Segelstad (1979) and Anthony et al. (1989) are similar but not identical to that of the present study. Due to extensive road alterations at the principal sampling site during the previous decade, not all the samples in the lowermost part of the Skien sequence necessarily correlate directly (e.g., S07 – Segelstad (1979) – and SK 07 – Anthony et al. (1989) – versus SKX 07 – this study).

Results

The chemistry of the Skien pyroxenes should be studied and interpreted in the light of the petrography of the overall lava sequence. The main sequence of lavas at Skien consists of approximately 70 nephelinite, tephrite and alkali basalt flows, numbered SKX 01–70 from base to top. A cross section and stratigraphic column are shown in Segalstad (1979). Further south, an additional, smaller road-cut sequence, just north of Porsgrunn (Fig. 1), contains pyroxene-phyric flows which have been numbered SKX 80–90. Their exact stratigraphic relationship with the main 70-flow Skien sequence is currently unclear but they appear to bear closest resemblance to flows around SKX 10–15. North of the main Skien basalts, a small block of pyroxene-phyric meta-basalt flows (SRX 1–6) are found near Skrim (Fig. 1) which are again believed to be related to the Skien basalts.

The majority of the lower flows in the main sequence, and all of the flows in the additional sequence are clinopyroxene-phyric, grading into clinopyroxene-plagioclase-phyric towards the upper end of the main sequence. Rare medium-coarse-grained, resorbed and altered olivine (Fo 85–87) has been found in three samples at the base of the main sequence. Partitioning calculations based on whole-rock data from these samples ($Mg\# = 100 \times Mg/(Mg + Fe) \approx 69$) as well as experimental data from Roedder and Emslie (1970) suggest that these olivine crystals are early phenocrysts. Flow SKX 40 (Mg# 56) contains Fo 89–90 olivine cores with 0.37–0.41% NiO which are overgrown by Fo 72–75 rims. The latter composition also forms rare, late-stage olivine phenocrysts within the sample. The cores are interpreted as xenocrysts whereas the rims and groundmass phenocrysts are considered to be cognate. The first appearance of plagioclase within the Skien sequence is in the groundmass of flow 40 (An 62), and it reappears in flows 55 and above, with more sodic compositions analyzed in flow 55 (~An 40). It forms a phenocryst phase in flows in the upper 50s and early 60s where it is too altered to yield reproducible analyses. Apatite, resorbed titanite, melanite garnet, nepheline and iron-oxide minerals are also found as groundmass phases in many of the Skien lavas (Segalstad 1979; this study).

Clinopyroxene petrography and major-element chemistry

Clinopyroxene is abundant and petrographically heterogeneous in the Skien lavas, and occurs in a variety of textural and compositional varieties (Table 1, Fig. 2). The major- and trace-element composition of representative samples from each of the different compositional types are given in Table 2, and illustrated graphically in Figs. 3 and 4. They are listed and described below according to their composition.

1. Cr-diopside cores (CrMgDi). These unzoned, bright green cores often show evidence of dissolution around the edges, and are always mantled with later generations of pyroxene (Fig. 2a). Such cores have been found in seven flows: SKX 07, 11, 31, 40, 44, 55 and 89A. Compositionally, these cores are distinct in Cr_2O_3-Mg

Table 1 Relationships between texture and composition for pyroxenes from the Skien basalts

Compositional type		Textural type	
CrMgDi	Cr-diopside MgO > 16 wt% Cr_2O_3 > 0.9 wt%	Xenocrystic core	Unzoned anhedral-subhedral distinct core of crystal, overgrown with concentrically zoned clinopyroxene (Fig. 2a)
	Cr-rich PhenDi MgO = 14.7–15.1 wt% Cr_2O_3 = 0.6–1.0 wt%	Overgrowth	Late-stage overgrowth rim in SKX 87 (Fig. 5) and rarely elsewhere
MgDi	Mg-rich, Cr-poor diopside MgO > 16 wt% Cr_2O_3 < 0.8 wt%	Mottled core	Resorbed mottled core, often with indistinct boundaries due to reaction with host melt
		"Clusters"	Glomeroporphyritic clusters of unzoned but sometimes twinned crystals, often sub/euhedral. Rare, most common in SKX 07
		"Strained"	Anhedral crystals showing strained extinction (only SKX 07)
PhenDi	Moderately Mg-rich (14–15.5 wt% MgO)	Phenocryst	Less resorbed/mottled cores, with core edges in equilibrium with rims. Concentric zones of diopside may periodically appear in broad rim dominated by Ti-augite
Ti-augite	Si-poor (45–48 wt% SiO_2) Ti-rich (2–4 wt% TiO_2) Mg-poor (10.5–14 wt% MgO)	Rims	Concentrically and sector-zoned rims found around xenocrystic, mottled or phenocrystic cores (Fig. 2a, d)
		"Strained"	Euhedral crystals (often megacrysts) which also show strained extinction as well as strong sector zonation
		Groundmass	Groundmass crystals

space (Fig. 3c). The most Mg-rich compositions ($\leq$18 wt% MgO) are found in sample SKX 11 (Fig. 4a–c). The Cr-diopside cores are also characterized by low Na, Al and Ti contents, and hence contain low proportions of jadeite and Tschermak components.

2. Mg-rich, Cr-poor diopside compositions (MgDi). These are often bright green (depending on their Cr contents), and have been found in a greater number of flows than the Cr-diopside cores (SKX 04, 05, 07, 14, 20, 27, 37B, 38, 40, 41, 55, 87, 89A and 89B). Compositionally, they have a wider range of Mg (16–17.5 wt% MgO) and lower Cr (0.1–0.8 wt% Cr_2O_3) contents but a higher content of Tschermak components than the Cr-diopside cores described above (Figs. 3, 4). Variation in Al/Ti ratios is also common within the suite (Fig. 4d).

MgDi compositions are most commonly found as parts of mottled crystal cores (e.g., Fig. 5), and most likely represent an example of the earliest stage of pyroxene crystallization within the magmas, or they are xenocrysts which have, in some samples, been subjected to varying degrees of dissolution by their host melts. MgDi compositions are also found, particularly in sample SKX 07, forming glomeroporphyritic clusters of unzoned clinopyroxene crystals, some of which are twinned, and which are rarely overgrown by later generations of pyroxene growth. The compositions of the glomeroporphyritic crystals are plotted in Fig. 3 as "cluster" analyses, and have low Al/Ti ratios compared with most of the other MgDi analyses. Sample SKX 07 is also host to rare anhedral crystals showing strained extinction and containing MgDi zones which are not mottled or resorbed (Fig. 2c). These analyses have been plotted as part of the "strained" group in Fig. 3, and again overlap the main MgDi compositions.

3. PhenDi. Yellow/green diopside forms either unresorbed phenocryst cores or diopsidic zones within concentrically zoned Ti-augite rim overgrowths (e.g., thin white zone in Fig. 2a). Compositionally, these diopsides have lower Mg and higher Tschermak contents than the MgDi compositions (Fig. 3). Their aegirine contents remain low (1.5–4%; Fig. 3f) whereas their Cr contents are very varied (0.0–1.1 wt% Cr_2O_3). The high-Cr compositions are found occasionally as late-stage resorption rims, or overgrowth rims believed to be formed as a result of magma mixing (Fig. 5), prior to final Ti-augite rim crystallization. The diopsides form a compositional continuum between the MgDi compositions and the Ti-augite overgrowths with MgO contents ranging from 14 to 16 wt%. The boundaries between the compositional groupings have been determined on the basis of both textural and compositional constraints.

4. Ti-augite. This, the most common type of pyroxene in these samples, is identified easily by its dark brown colour in hand specimen, and pale pink-brown colour in plane-polarized-light. Although a few samples contain Ti-augite phenocrysts (e.g., SKX 70; Fig. 2d), the composition is most commonly found as concentrically zoned overgrowths on earlier-formed core compositions (Fig. 2a, c), and as groundmass crystals. Ti-augite also forms rare euhedral megacrysts in a few samples, some of which show strained extinction, and are plotted as part of the "strained" group in Fig. 3. Compositionally, the Ti-augites have the lowest MgO (10–14 wt%) and highest Tschermak contents of all the pyroxene types in the Skien lavas (Fig. 3). Their aegirine contents range from $\sim$1.5 to 6% (Fig. 3f).

Geothermobarometry

The major element data from the four pyroxene types described above were used to estimate pressures and temperatures of crystallization, using the statistical clinopyroxene geothermobarometer of Soesoo (1997).

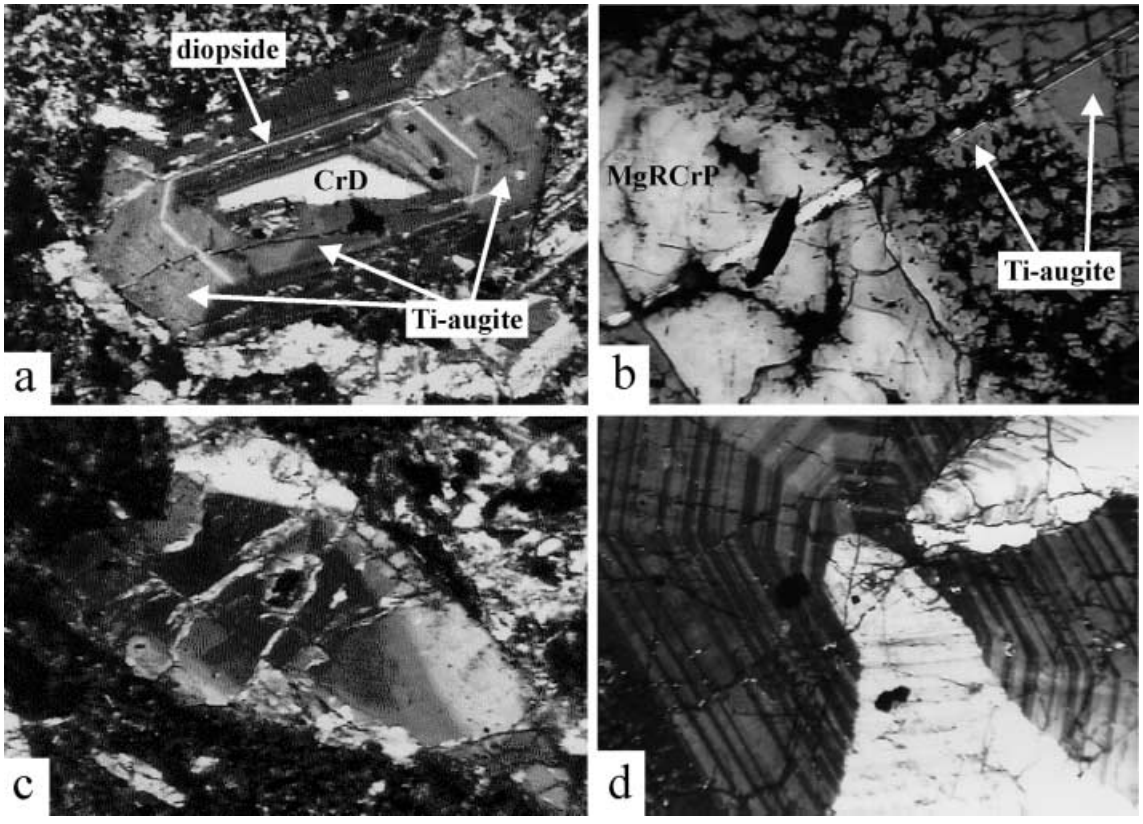

Fig. 2 Photomicrographs (cross-polarized light) of clinopyroxenes from the Skien lavas, showing the four main compositional types. The field of view for all panels is 2 mm wide. **a** Clinopyroxene from sample SKX 07. The unzoned (white) clinopyroxene core is Cr-diopside, and is overgrown by concentrically and sector-zoned Ti-augite. The thin white concentric zone appearing approximately a third of the way out from the core (in the Ti-augite overgrowth) has a PhenDi composition. **b** Clinopyroxene crystal from sample SKX 14, with a Mg-rich, Cr-poor core (MgDi) exhibiting mottled zonation and evidence of dissolution. The core is overgrown by an extensively remelted zone, essentially Ti-augite in composition, and finally by a smoother, homogeneous Ti-augite rim. **c** Anhedral MgDi-rich pyroxene from sample SKX 07 which shows strained extinction. **d** Concentrically and sector-zoned phenocryst of Ti-augite containing no other type of core material (from sample SKX 70)

The results are plotted in Fig. 3f, and suggest that the Ti-augite compositions crystallized between approximately 1,100 and 1,150 °C, and at relatively low pressures (< 3 kb) whereas the PhenDi compositions lie within the 2–5 kbar and 1,150–1,200 °C field. However, the CrMgDi and MgDi compositions lie outside the range of the field of calibration of the Soesoo (1997) geothermobarometer. The clinopyroxene geothermobarometer from Putirka et al. (1996), which is based on the composition of clinopyroxene and co-existing liquid, was used to estimate pressure and temperature of crystallization of the MgDi compositions from sample SKX 14, which is the most primitive lava found at Skien. The calculations gave pressures of ~12 kbar and temperatures of ~1,250 °C. The Putirka et al. (1996) geothermobarometer is not calibrated for Fe^{3+}-rich clinopyroxenes, and was not used to calculate PT crystallization conditions for any of the PhenDi or Ti-augite compositions.

Clinopyroxene trace-element geochemistry

Five samples, containing a wide and representative variety of the clinopyroxene types described above, were selected for pyroxene trace-element ion-probe analysis (SKX 07, 11, 14, 44, 70). Representative results are provided in Table 2, and data from the first four samples are plotted as mantle-normalised spider-diagrams in Fig. 6a–d, along with the whole-rock spidergram for each sample.

It is clear from Fig. 6a–d that the different generations of clinopyroxene within each sample are not in equilibrium with respect to trace-element composition, and that the large-ion-lithophile-elements (LILE) in particular show very inconsistent behaviour. The Ti-augite trace-element compositions (overgrowths, and "strained" in SKX 14) are commonly more trace-element-enriched than the related host rock.

A comparison of average trace-element compositions for different types of Skien pyroxene (listed in Table 2) is plotted in Fig. 6e. Particularly noteworthy are the extremely homogeneous trace-element compositions of the Ti-augite throughout the Skien sequence, the relatively close similarity in trace-element signatures between the CrMgDi and MgDi compositions, the similarity in composition between the MgDi cores and

Table 2 Average clinopyroxene compositions of representative samples of the pyroxenes shown in Figs. 3–6. Major-element data (wt%) obtained using a Camebax microprobe. Analyses normalised with 4 cations:6 oxygens; Fe^{3+} calculated by charge-balance. Trace-element data (ppm) determined by Caméca ion probe (see Analytical methods for further details). "Avg. (7/3)" indicates the average of the number of major-element and trace-element analyses, respectively

Pyx-type	Cr-diopside (CrDi)			Mg-rich, Cr-poor (MgDi)				
Sample								
No. analyses (major/trace)	SKX 07 Avg. (1/1)	SKX 11 Avg. (3/2)	SKX 44 Avg. (3/3)	SKX 07 Avg. (14/5) (cluster)	SKX 07 Avg. (4/3) (strained)	SKX 14 Avg. (1/2)		
SiO_2	53.18	53.61	52.55	52.96	52.53	52.99		
TiO_2	0.61	0.45	0.60	0.73	0.81	0.58		
Al_2O_3	1.67	1.21	2.36	1.67	2.10	2.13		
Cr_2O_3	1.07	0.99	1.07	0.57	0.41	0.51		
Fe_2O_3	0.59	0.43	1.40	0.60	1.53	0.76		
FeO	2.84	2.83	3.01	3.61	3.29	3.13		
MnO	0.06	0.06	0.08	0.09	0.09	0.05		
MgO	16.67	17.47	16.27	16.21	16.00	16.39		
NiO	0.10	0.07	0.04	0.05	0.10	b.d.		
CaO	23.37	22.41	22.57	23.25	23.04	23.01		
Na_2O	0.32	0.37	0.50	0.32	0.44	0.42		
K_2O	b.d.	0.02	0.02	0.03	0.02	0.02		
Total	100.48	99.91	100.47	100.08	100.36	99.99		
Si	1.935	1.955	1.916	1.941	1.921	1.936		
^{iv}Al	0.065	0.045	0.084	0.059	0.078	0.064		
$^{iv}Fe^{3+}$		0.001			0.005			
^{vi}Al	0.007	0.011	0.018	0.013	0.017	0.028		
$^{vi}Fe^{3+}$	0.016	0.011	0.039	0.018	0.041	0.021		
Ti	0.017	0.012	0.016	0.020	0.022	0.016		
Cr	0.031	0.028	0.031	0.017	0.012	0.015		
Fe^{2+}	0.086	0.086	0.092	0.111	0.101	0.096		
Mn	0.002	0.002	0.002	0.003	0.003	0.002		
Mg	0.904	0.950	0.884	0.885	0.872	0.893		
Ni	0.003	0.002	0.002	0.001	0.003			
Ca	0.911	0.876	0.882	0.913	0.903	0.901		
Na	0.023	0.026	0.035	0.023	0.031	0.030		
K				0.002	0.001			
Total	4.000	4.000	4.000	4.000	4.000	4.000		
Ba	0.15	0.37	0.33	0.56	1.16	0.42		
Th	0.038	0.010	0.021	0.016	0.020	0.024		
U	0.051	0.032	0.028	0.015	0.055	0.011		
Nb	0.21	0.19	0.28	0.20	0.16	0.16		
Sr	94.2	100.2	78.2	114.6	117.3	96.5		
Zr	10.07	6.2	8.6	13.3	15.8	13.2		
Hf	0.35	0.22	0.33	0.69	0.91	0.72		
Ti	3148	2168	2919	3732	4003	3745		
Y	2.65	1.63	3.30	4.60	5.18	3.01		
La	2.23	2.04	1.73	3.21	3.27	2.19		
Ce	7.63	6.16	5.44	10.43	10.74	7.16		
Pr	1.17	0.99	0.90	1.82	1.95	1.30		
Nd	6.35	4.94	6.01	9.36	10.23	7.37		
Sm		1.08	1.55	2.07	2.65	1.81		
Eu		0.33	0.50	0.68	0.69	0.56		
Gd	1.40	0.66	1.12	1.43	1.36	1.48		
Tb	0.11	0.08	0.14	0.23	0.23	0.19		
Dy	0.85	0.52	1.00	1.13	0.94	0.76		
Ho	0.09	0.06	0.12	0.19	0.16	0.12		
Er	0.23	0.13	0.32	0.45	0.49	0.37		
Tm	0.04	0.026	0.049	0.053	0.074	0.045		
Yb	0.39	0.30	0.35	0.67	0.86	0.33		
Lu	0.03	0.009	0.025	0.038	0.100	0.032		
Pyx-type	Phenocryst diopside (PhenDi)			Ti-augite				
Sample								
No. analyses (major/trace)	SKX 01 Avg. (8)	SKX 07 Avg. (3)	SKX 11 Avg. (1/1)	SKX 07 Avg. (7/1)	SKX 11 Avg. (3/2)	SKX 14 Avg. (9/6)	SKX 44 Avg. (7/4)	SKX 70 Avg. (27/5)
SiO_2	50.72	51.37	51.48	48.54	46.92	46.24	47.80	44.19
TiO_2	1.27	1.36	0.94	2.35	2.24	2.81	2.35	3.45
Al_2O_3	3.67	2.65	2.93	4.68	6.24	6.74	5.89	8.91
Cr_2O_3	0.40	0.31	0.28	0.07	0.09	0.08	0.03	0.06

Table 2 (Contd.)

Pyx-type	Phenocryst diopside (PhenDi)			Ti-augite				
Sample								
No. analyses (major/trace)	SKX 01 Avg. (8)	SKX 07 Avg. (3)	SKX 11 Avg. (1/1)	SKX 07 Avg. (7/1)	SKX 11 Avg. (3/2)	SKX 14 Avg. (9/6)	SKX 44 Avg. (7/4)	SKX 70 Avg. (27/5)
Fe_2O_3	1.55	1.98	1.57	3.54	4.22	3.98	3.16	4.27
FeO	2.63	3.87	3.84	4.16	3.21	4.12	4.47	4.37
MnO	0.06	0.10	0.11	0.16	0.09	0.14	0.17	0.15
MgO	14.93	15.26	15.45	13.60	12.94	12.00	12.72	11.10
NiO	0.05	0.07	0.08	0.06	0.03	0.03	0.03	0.03
CaO	24.41	23.22	22.52	22.63	22.82	23.14	22.83	22.43
Na_2O	0.25	0.36	0.42	0.55	0.53	0.53	0.57	0.62
K_2O	0.02	0.01	0.01	0.02	0.02	0.02	0.02	0.01
Total	99.96	100.55	99.63	100.34	99.35	99.83	100.03	99.58
Si	1.867	1.886	1.900	1.802	1.758	1.735	1.781	1.666
^{iv}Al	0.133	0.113	0.100	0.196	0.242	0.265	0.219	0.334
$^{iv}Fe^{3+}$		0.002		0.006				
^{vi}Al	0.026	0.002	0.027	0.012	0.034	0.033	0.040	0.062
$^{vi}Fe^{3+}$	0.043	0.054	0.044	0.097	0.119	0.112	0.089	0.121
Ti	0.035	0.038	0.026	0.066	0.063	0.079	0.066	0.098
Cr	0.012	0.009	0.008	0.002	0.003	0.003	0.001	0.002
Fe^{2+}	0.081	0.119	0.119	0.129	0.101	0.129	0.140	0.138
Mn	0.002	0.003	0.003	0.005	0.003	0.004	0.005	0.005
Mg	0.819	0.835	0.850	0.753	0.723	0.671	0.707	0.624
Ni	0.002	0.002	0.002	0.002	0.001	0.002	0.001	0.001
Ca	0.963	0.914	0.890	0.900	0.916	0.930	0.912	0.906
Na	0.018	0.026	0.030	0.040	0.039	0.039	0.041	0.045
K								
Total	4.000	4.000	4.000	4.000	4.000	4.000	4.000	4.000
Ba			0.28	0.59	0.99	1.23	0.63	0.71
Th			0.05	0.06	0.168	0.176	0.180	0.196
U			0.01	0.05	0.030	0.033	0.032	0.021
Nb			0.37	1.50	1.86	2.45	2.29	2.57
Sr			119.5	230.9	252.9	264.8	251.7	226.9
Zr			46.52	156.27	184.7	231.7	242.3	216.7
Hf			2.07	6.53	6.70	7.75	8.75	7.33
Ti			8,088	12,974	14,464	16,166	17,322	15,975
Y			6.45	19.28	17.04	19.95	22.60	18.17
La			5.16	18.35	18.45	21.28	22.11	19.64
Ce			17.35	58.04	57.33	66.04	68.00	63.00
Pr			2.95	9.31	9.53	10.86	11.03	10.56
Nd			16.04	45.61	46.04	55.02	57.42	52.95
Sm			3.80	9.33	10.35	11.22	11.95	11.33
Eu			1.23	2.47	3.15	3.15	3.72	3.24
Gd			1.82	7.00	4.53	7.70	7.64	6.54
Tb			0.32	0.85	0.78	1.02	1.25	0.93
Dy			1.57	4.80	3.95	5.07	5.43	4.32
Ho			0.22	0.71	0.68	0.79	0.86	0.68
Er			0.51	1.84	1.50	1.78	1.94	1.63
Tm			0.07	0.282	0.160	0.229	0.162	0.190
Yb			0.46	1.52	1.59	1.57	1.34	1.38
Lu			0.03	0.121	0.123	0.170	0.182	0.147

twinned glomeroporphyritic MgDi compositions from sample SKX 07, and the clear differences between the Ti-augite and Mg-rich diopsidic trace-element patterns, especially with respect to REE, Zr and Hf contents. As expected, the single PhenDi analysis from sample SKX 11 lies between the Ti-augite and MgDi analyses. Despite their general similarity, there are some consistent differences between the CrMgDi and MgDi compositions, particularly with respect to Hf^*_N (where $Hf*_N = Hf_N - (Zr_N + Ti_N)/22$) which is consistently positive in the MgDi compositions, and negative in the Cr-diopside cores.

Also shown in Fig. 6e is the calculated composition of clinopyroxene in equilibrium with the whole-rock composition of sample SKX 14 at 3 GPa and 1,380 °C, using partition coefficients taken from Hart and Dunn (1993; Table 3). SKX 14 is one of the most primitive lavas found at Skien (Mg#~61; $Al_2O_3 = 10.8$ wt%; Cr = 270 ppm; $Mg\# = 100 \times Mg/(Mg + Fe_T)$), with the lowest REE contents. The calculated pyroxene composition lies between that of the PhenDi and MgDi analyses and is believed to be representative of the earliest cognate pyroxenes, although earlier fractionation may have enriched the trace-element composition

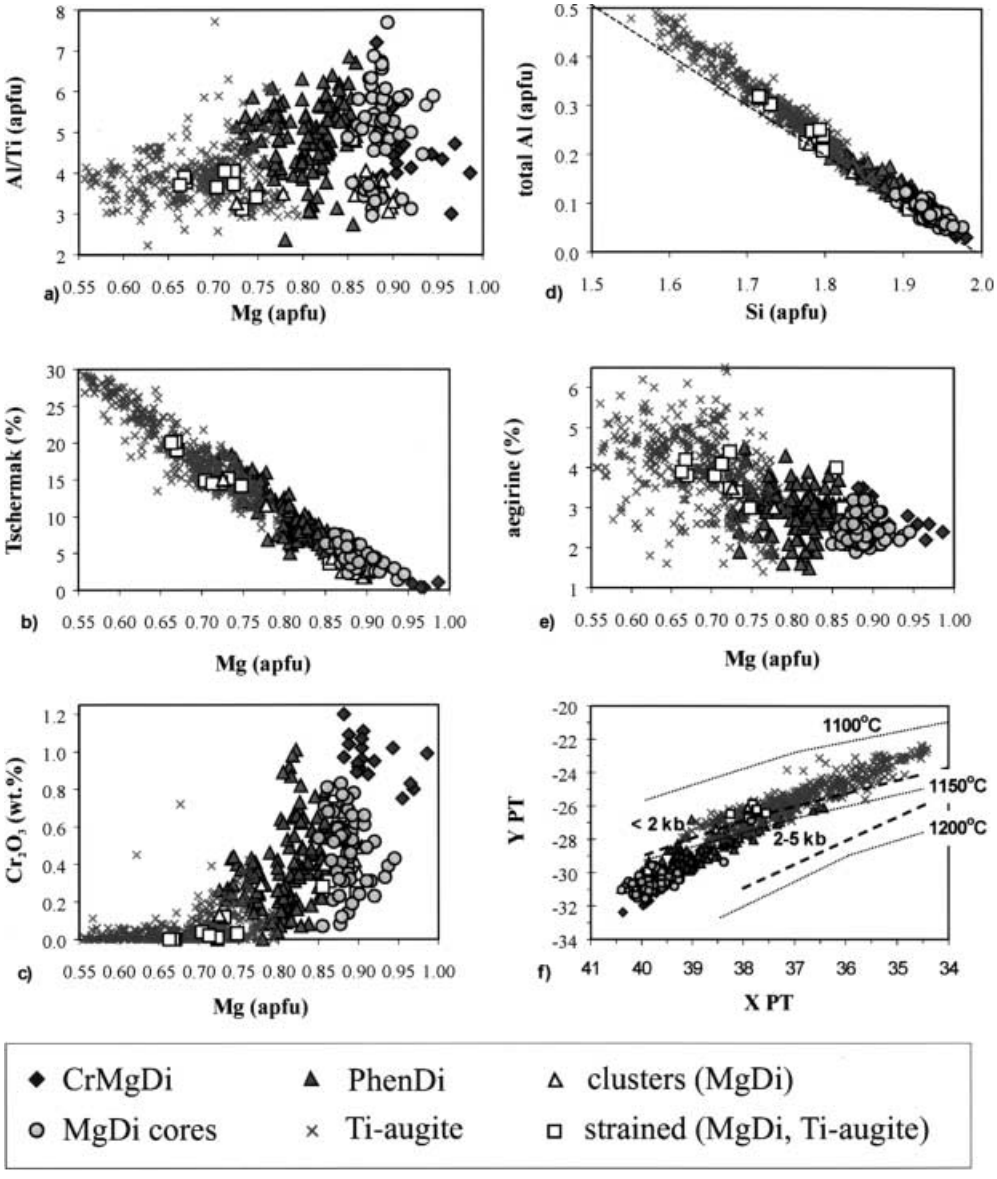

Fig. 3a–f Major-element and pyroxene-component plots showing the compositions of the different types of clinopyroxene found in the Skien lavas, as defined in this study on the basis of petrographic and compositional data. ''Tschermak'' includes the combined calculated presence of the components $CaAl_2SiO_6$, $CaFe^{3+}AlSiO_6$, $CaFe^{3+}{}_2SiO_6$, and $CaTiAl_2O_6$. Na has been assumed to be present in the aegirine component. The ''cluster'' analyses refer to glomeroporphyritic associations of mostly MgDi crystals in sample SKX 07. ''Strained'' crystals are those which exhibit obvious strained extinction. They include an anhedral MgDi crystal from sample SKX 07, and euhedral Ti-augite crystals from samples SKX 14 and 44. Figure 3f shows calculated pressure-temperature crystallization conditions for the pyroxenes based on the statistical multivariate calculations of Soesoo (1997). $)X_{PT} = 0.446SiO_2 + 0.187TiO_2 - 0.404Al_2O_3 + 0.346FeO(tot) - 0.052MnO + 0.309MgO + 0.431CaO - 0.466Na_2OO$. $OY_{PT} = -0.369SiO_2 + 0.535TiO_2 - 0.317Al_2O_3 + 0.323FeO(tot) + 0.235MnO - 0.516MgO - 0.167CaO - 0.153Na_2OO$. This geothermobarometer was calibrated for 338 experimental analyses ranging from 1 atm to 34 kbar and 1,000–1,470° C, and subsequently tested using several hundred natural analyses from mafic rocks, mostly from the oceanic environment, whose petrographic histories are well constrained

of sample SKX 14 relative to the original, primitive magma. However, given the whole-rock Mg# of 61, we do not believe that the whole-rock composition has undergone substantial fractionation, and thus the ''calculated pyroxene'' composition cannot be substantially more enriched than the true values of the earliest cognate pyroxenes. It must be noted that the CrMgDi compositions are substantially more depleted in most elements, particularly in Zr-Hf, than the ''calculated pyroxene'' composition.

The consistency of the Ti-augite trace-element compositions supports the assertion that these pyroxenes were in equilibrium with their host melts during late-stage magma crystallization. In turn, this observation has allowed us to calculate Ti-augite/melt partition coefficients (D) for each sample using both whole-rock compositions as well as groundmass compositions estimated by point-counting and stripping the earlier diopside growth compositions from the

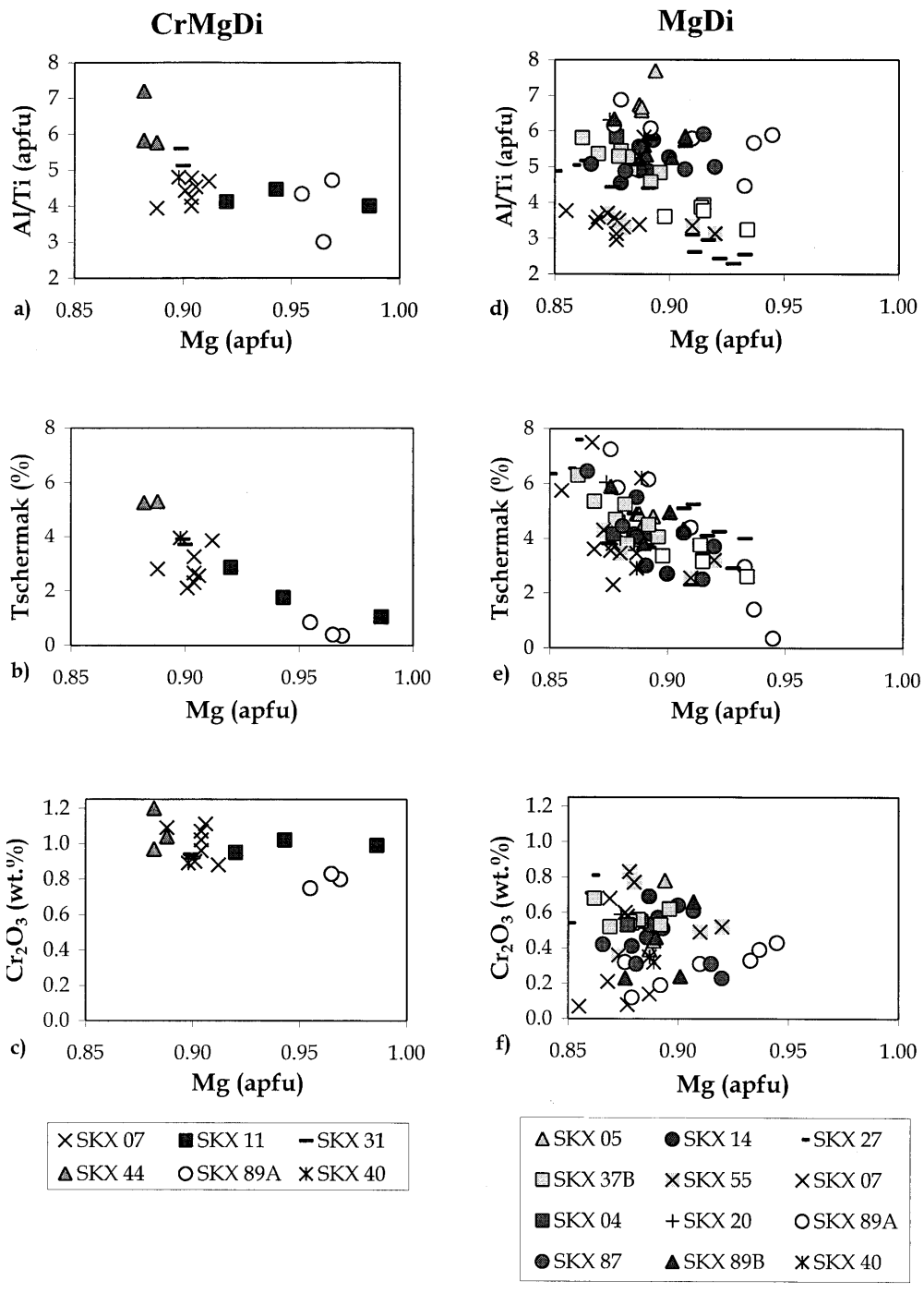

Fig. 4 **a–c** Compositions of Cr-diopside cores (CrMgDi) as used in Fig. 3, plotted according to sample number. Sample SKX 11 contains the most depleted (high-Mg, low-Tschermak) xenocryst compositions of all samples analyzed. The low-Mg, high-Cr analysis from sample SKX 11 comes from the rim of a xenocryst core, and may represent the result of xenocryst reaction with the host melt. **d–f** Compositions of Mg-rich, Cr-poor diopside cores (MgDi) as used in Fig. 3, plotted according to sample number. The graphs do not include the "cluster" and "strained" analyses from sample SKX 07 which have compositions similar to the MgDi analyses from the same sample

whole-rock analyses. These D values are listed in Table 3 and plotted in Fig. 6f along with clinopyroxene partition coefficients taken from the literature. Our results show that, during the late stages of crystallization at approximately 1,100–1,160 °C and < 2 kb (Fig. 3f), most elements more "compatible" than Nd are compatible in Ti-augite. Our calculated values show closest resemblance to those of Francalanci et al. (1989), which were calculated for similar compositions under similar crystallization conditions and which are substantially higher than those calculated for pyroxenes crystallizing under high temperature and pressure conditions. The samples analyzed in this study for pyroxene trace-element compositions are solely pyroxene-phyric, and contain no plagioclase or significant quantities of other minerals that might affect trace-element partitioning, with the exception of Ti partioning into minor amounts of groundmass magnetite. Crystallization of minor amounts of magnetite prior to the formation of the Ti-augite compositions would mean that our calculated D_{Ti} values are minimum values.

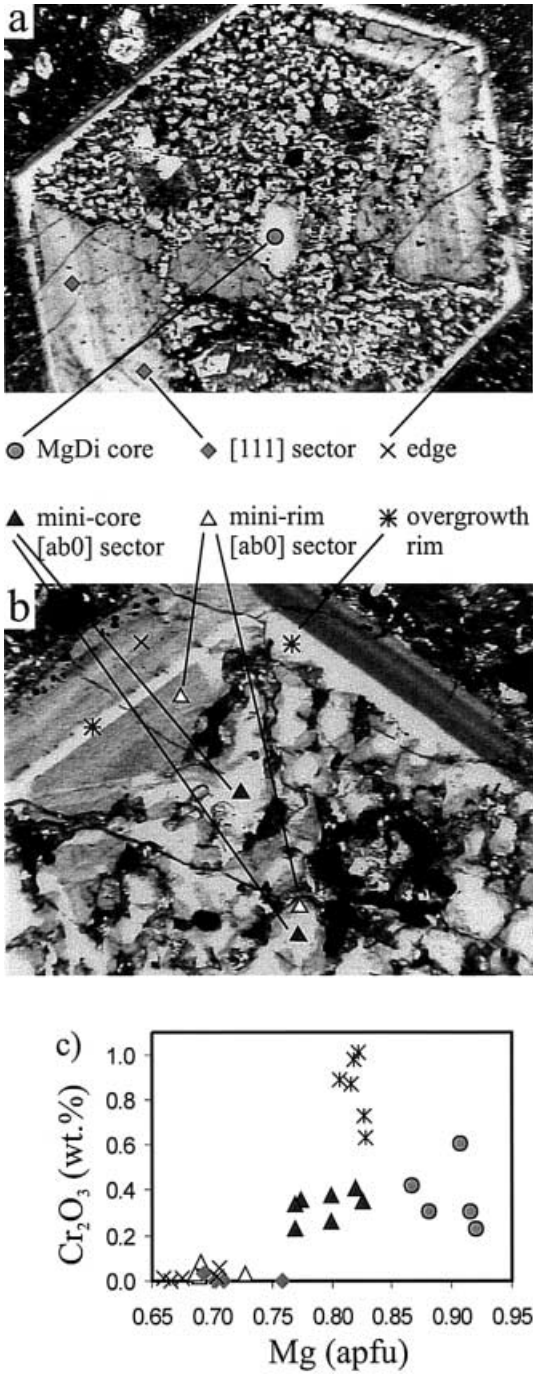

Fig. 5 Clinopyroxene crystal from sample SKX 87 exhibiting an MgDi core overgrown by Ti-augite, and subjected to subsequent sector-selective dissolution processes. The partially melted [ab0] and relatively intact [111] sectors are overgrown by a concentric zone of Cr-rich, Mg-poor diopside, and finally Ti-augite. **a** Crossed-polars view of the 2-mm-diameter crystal. **b** Close-up of one of the crystal apices shown in **a** above. **c** Compositional demonstration of the relationships between texture and chemistry. Symbols as shown in **a** and **b** above

Sr-Nd isotope geochemistry

In order to test if the chemical and petrographic disequilibrium corresponds with disequilibrium previously reported in the radiogenic isotope systems (Anthony et al. 1989), Rb-Sr and Sm-Nd isotopic analyses were conducted on pyroxene separates and related whole-rock powders. The pyroxenes were handpicked according to colour (bright green = Cr-rich (CrMgDi or MgDi), yellow-green = PhenDi, and brown = Ti-augite) and subsequently powdered. All powders were leached according to the procedures described above (cf. Analytical methods). The results are given in Table 4. Data for the leached whole-rock powders and pyroxenes, along with nonleached whole-rock and pyroxene analyses from Anthony et al. (1989), are shown in Fig. 7. The differences in the Rb/Sr (and Sm/Nd) ratios between leached and nonleached whole-rock and pyroxene analyses, and the subsequent effects on the age-corrected isotope ratios (Table 4) are discussed in detail below.

The combined pyroxene and whole-rock initial-ratio isotope data (Fig. 7a) demonstrate clear intrasample disequilibrium between the different generations of pyroxene and their host magmas, particularly in the leached samples. The reasons for pyroxene-whole-rock disequilibrium may be due to alteration of parent-daughter ratios

►

Fig. 6 **a–d** Mantle-normalised spidergrams of trace-element data from different types of pyroxenes in samples SKX 07, 11, 14 and 44. Also shown for comparison is the whole-rock composition for each of the samples (WR). Mantle normalisation factors were taken from McDonough and Sun (1995). **a** The "cluster" analyses in sample SKX 07 are from the same crystals as those whose major-element data are plotted in Fig. 3. There is one Cr-diopside analysis (*CrMgDi*; core in Fig. 2a), two analyses of a MgDi crystal showing strained extinction (*strained*; Fig. 2b) whose major-element data is also plotted as "strained" samples in Fig. 3, and one analysis of a Ti-augite overgrowth rim. **b** Analyses from sample SKX 11 include two from the most Mg-rich Cr-diopside core plotted in Fig. 3 (*CrMgDi*), and three from the overgrowth rim around the core. The first of these is from a diopside zone, while the other two are taken from Ti-augite zones. **c** Sample SKX 14 data include two MgDi core analyses and two Ti-augite overgrowths taken from the crystal shown in Fig. 2b, and "strain" analyses from a sheared, euhedral Ti-augite megacryst. **d** The three trace-element-depleted xenocryst-core analyses (*CrMgDi*) and two overgrowth analyses (*Ti-augite*) shown in this plot are from a single crystal in sample SKX 44. The "megacryst" analyses are taken from a nonsheared, sector-zoned Ti-augite megacryst, approximately 2 cm in diameter. **e** Average trace-element data for Cr-diopside cores (*CrMgDi*), MgDi (including "strained" and "cluster" analyses from samples SKX 07), and Ti-augites. Note the consistency of the Ti-augite compositions, the depleted nature of the Cr-diopside and MgDi compositions, and the differences in Hf_N* between the Cr-diopside and MgDi averages ($Hf_N^* = Hf_N - ((Zr_N + Ti_N)/2)$). Also plotted is the calculated composition (calc pyx) of clinopyroxene crystallizing in equilibrium with a melt of the whole-rock composition of sample SKX 14 (one of the most primitive lavas found at Skien) at 3 GPa and 1,380° C, calculated using pyroxene/melt coefficients from Hart and Dunn (1993). **f** Calculated Ti-augite/melt partition coefficients (D) for the Skien samples (cf. Table 3), based on the average Ti-augite compositions from the five samples analyzed (cf. Table 2). The D values for the middle and heavy rare earth elements, Zr, and Hf are greater than unity. Other relevant partition coefficients from the literature are shown for comparison (cf. Table 3), along with their pressure and temperature of measurement (where known). The calculated error bars are normally smaller than the symbols used for each data point

through the leaching process. However, experimentation with leaching procedures during this study has shown that leaching of the pyroxene separates merely removes secondary alteration and does not affect the primary parent-daughter element ratios and the isotopic ratios. Thus, intrasample pyroxene disequilibrium is almost certainly a real characteristic of these samples. When plotted according to pyroxene or whole-rock types, there are systematic variations in the isotope data (Fig. 7b). The "green" pyroxenes (mostly PhenDi compositions) exhibit very similar $^{87}Sr/^{86}Sr_i$ but varied $^{143}Nd/^{144}Nd_i$ signatures, whereas the brown (Ti-augite) and whole-rock analyses show similar Nd but varied Sr signatures. The lone MgDi analysis comes from sample SKX 37B.

Work is currently in progress to fully characterize the Sr-Nd-Pb isotopic signatures of the different pyroxene types within the Skien basalts and other B1-sequence basalts elsewhere in the Oslo Rift.

Discussion

Ti-augite partition coefficients

Intrasample disequilibrium can cause difficulties in interpreting and modelling whole-rock data. In the case of the Skien basalts, the results above demonstrate that the characterization of such intrasample textural and

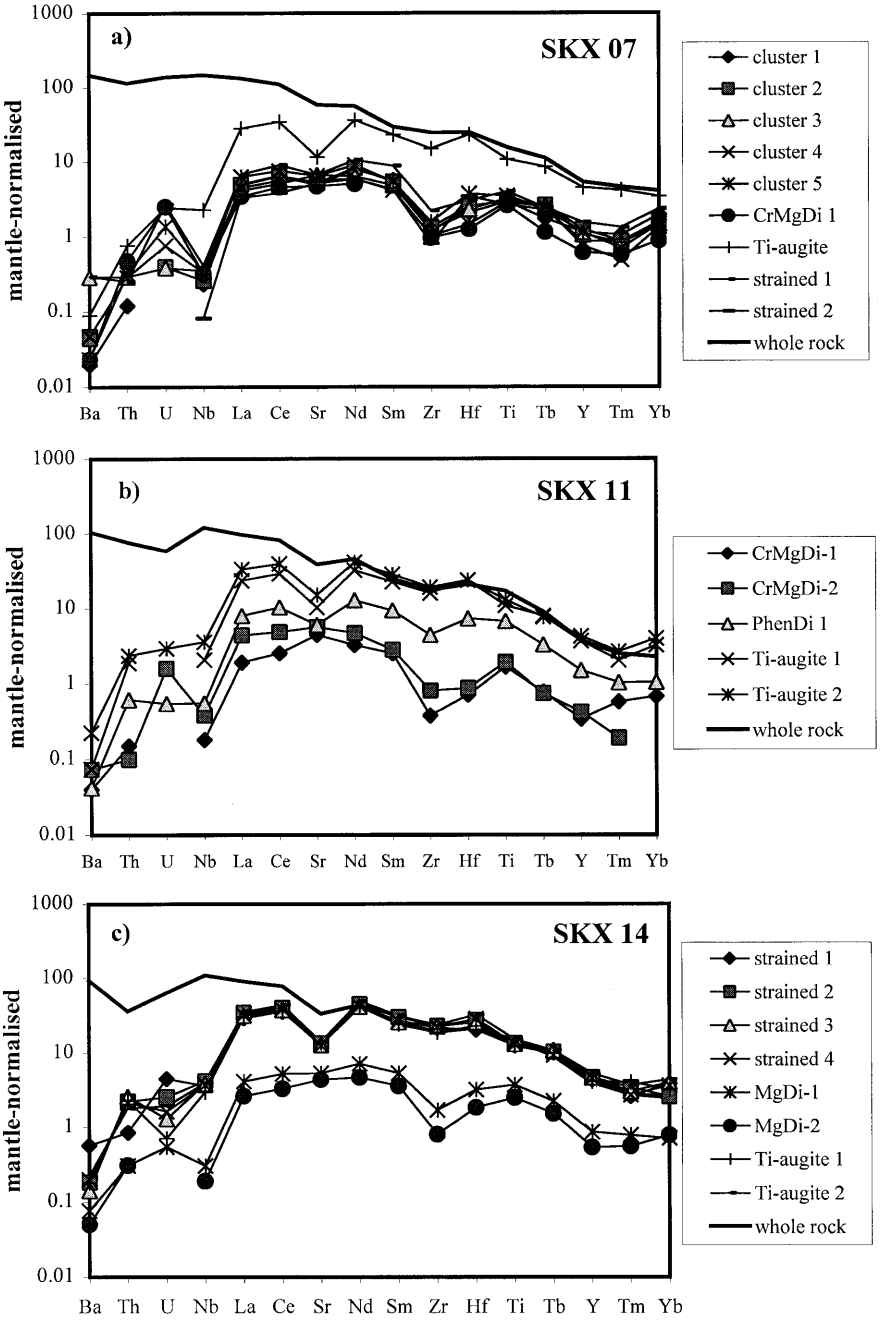

Fig. 6 (Contd.)

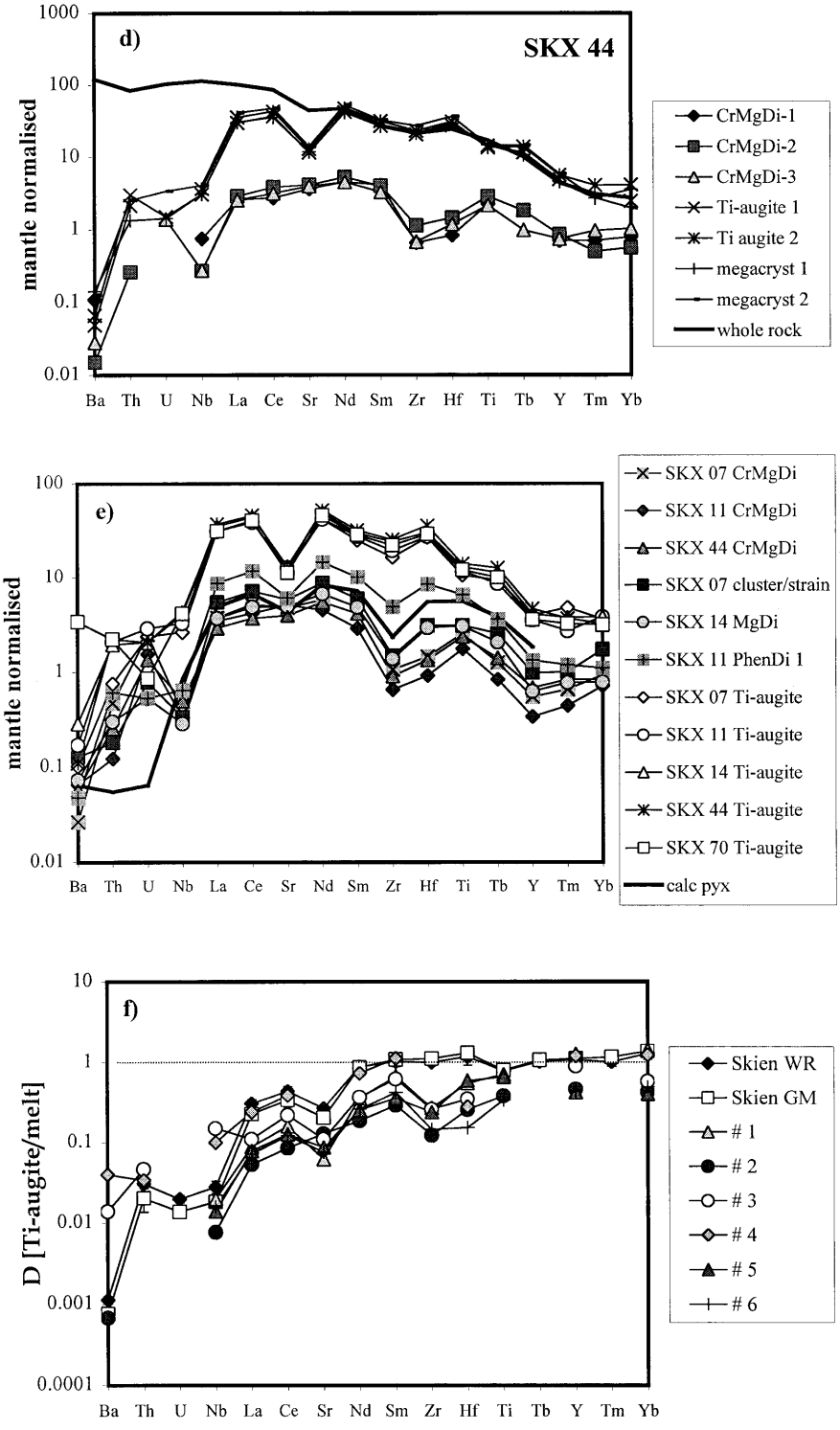

geochemical disequilibrium is necessary in order to unravel the complex magmatic history and evolution of these lavas. The data clearly show that the Ti-augite is the only generation of pyroxene growth in the Skien which may be considered to be in equilibrium with the host lava. This is consistent with their mode of occurrence asovergrowths around various types of diopsidic clinopyroxene. Specific intrasample equilibrium is not always seen in isotope space, but the isotope compositions of the whole-rock samples and Ti-augites overlap in a general sense, particularly with respect to ϵNd. Alteration effects and problems in accurately estimating the primary Rb/Sr parent-daughter ratios may account for the remaining discrepancies in the Sr isotopic system.

Table 3 Comparison of high-temperature magmatic partition coefficients for cpx/melt from this study and the literature. *WR* D = cpx/whole-rock. *GM* D = cpx/(estimated) groundmass. The six datasets extracted from the literature have the following T, P, and "melt" composition. *No. 1* 1,269 °C, 1.0 GPa, cpx-melt (sp. lherz. solidus; Blundy et al. 1998). *No. 2* 1,380 °C, 3 GPa, alkali basalt (Hart and Dunn 1993). *No. 3* T and P not available, shoshonite-basalt (Francalanci 1989). *No. 4* T and P not available, shoshonite (Francalanci 1989). *No. 5* 1,270 °C, 2.5 GPa, nephelinite (Skulski et al. 1994). *No. 6* 1,250 °C, 1.0 GPa, alk ol basalt (Skulski et al. 1994)

Sample	Average (WR)	SD (%)	Average (GM)	SD (%)	No. 1	No. 2	No. 3	No. 4	No. 5	No. 6
Ba	0.0011	10	0.0008	10		0.00068	0.01	0.04		
Th	0.031	22	0.020	22			0.05	0.03		
U	0.020	11	0.014	11						
Nb	0.028	18	0.018	18	0.02	0.0077	0.15	0.10	0.014	0.016
Sr	0.27	10	0.20	10	0.062	0.1283	0.11		0.087	0.076
Zr	1.0	9	1.1	9	0.27	0.1234	0.26		0.238	0.145
Hf	1.2	22	1.3	22	0.55	0.256	0.35	0.28	0.595	0.153
Ti	0.78	13	0.80	13	0.71	0.384			0.658	0.340
Y	1.1	7	1.1	7	1.27	0.467	0.90	1.20	0.426	0.442
La	0.31	12	0.23	12	0.089	0.0536	0.11	0.24	0.079	0.072
Ce	0.44	14	0.34	14	0.16	0.0858	0.22	0.39	0.127	0.122
Pr	0.68	15	0.59	15						
Nd	0.9	14	0.9	14	0.36	0.1873	0.37	0.73	0.255	0.260
Sm	1.0	13	1.1	13	0.67	0.291	0.62	1.12	0.359	0.421
Eu	1.0	10	1.0	10	0.38		0.59	1.22		
Gd	1.0	13	1.1	13	0.99					
Tb	1.0	14	1.1	14			0.58	1.38		
Dy	1.1	10	1.3	10		0.442			0.418	0.571
Ho	1.1	12	1.3	12						
Er	1.1	12	1.3	12	1.44	0.387				
Tm	1.0	13	1.2	13						
Yb	1.3	14	1.4	14	1.43	0.43	0.58	1.24	0.405	0.494
Lu	1.0	14	1.2	14	1.48	0.433	0.80	1.10		

The consistency of the Ti-augite trace-element compositions, and the Nd isotopic equilibrium between the whole-rock and Ti-augite data suggest that the calculated pyroxene/melt partition coefficients are geochemically reasonable for these lavas, bearing in mind that the middle and heavy rare earth elements (REE) as well as Zr, Hf and Y are compatible in Ti-augite formed under low pressures and basaltic magmatic temperatures (Neumann 1994). The large ion lithophile elements (LILE), Nb and Sr are incompatible, and Ti is only mildly incompatible.

D values were calculated using both whole-rock (WR) and estimated groundmass (GM) (assumed melt) compositions. The true Ti-augite D values should lie somewhere between these two extremes. D_{Ti} is particularly difficult to estimate accurately due to uncertainty in the relative timing of Ti-augite and groundmass magnetite crystallization. Early crystallization of the latter will affect the content of Ti in the calculated groundmass compositions used for the D-value calculations. The calculated D_{Yb} values are believed to be unrealistically high due to the large analytical uncertainty associated with low Yb contents.

Table 3 includes clinopyroxene/melt partition coefficients from Francalanci (1989), Hart and Dunn (1993), Skulski et al. (1994), and Blundy et al. (1998), chosen to represent diopsidic clinopyroxenes which have crystallized under a variety of PT conditions from mafic magmas. The D values from groundmass pyroxenes from shoshonitic lavas at Stromboli (Francalanci 1989) are particularly similar to the Skien Ti-augite data, although the Zr and Hf values calculated for the Skien Ti-augites are still significantly higher than those found in the other datasets, both in terms of absolute values and relative to elements with similar degrees of compatibility. The reasons for this are currently unclear, although the high Tschermak-component content of the Skien Ti-augites may explain the strong compatibility of these quatro-valent cations (Rocholl et al. 1996).

Origin of the Cr-diopside (CrMgDi) and MgDi compositions

There are currently three main hypotheses to explain the origins of the CrMgDi and MgDi compositions, these being (1) mantle xenocrysts, (2) partially melted mantle xenocrysts, or (3) early congnate phenocrysts.

Mantle xenocrysts

It is common to find Cr-diopsides in mantle lherzolite xenoliths brought to the surface within Si-undersaturated basalts (e.g., Nixon 1987). However, most lherzolite Cr-diopsides contain ≥1.0 wt% Na_2O along with significant amounts of ^{vi}Al to form the jadeite component, and have very low Ti contents (e.g., Frey and Prinz 1978; Nixon 1987). Such jadeite-rich Cr-diopsides are found in mantle xenoliths exhumed by silicate rocks in the nearby 580-Ma Fen carbonatite complex (Griffin 1973). The results of the present study show that neither

Table 4 Sr-Nd isotope results for selected Skien pyroxenes and whole-rock samples (leached whole-rock and pyroxene data plotted in Fig. 7; see Analytical methods section for details). The "leached/ICP-MS" whole-rock results use ICP-MS Rb, Sr, Sm and Nd concentration data, and the leached measured Sr and Nd isotope ratios to calculate the resultant initial ratios. Samples SKX 01, 49 and 55 also list nonleached isotope-dilution (ID) Rb, Sr, Sm and Nd concentrations, measured Sr and Nd isotope ratios, and the resultant calculated initial isotope ratios. Average of standard analyses carried out during this study: NBS 987 $^{87}Sr/^{86}Sr = 0.71024 \pm 1$ (VG 54) and JM $^{143}Nd/^{144}Nd = 0.51111 \pm 1$ (Finnegan-MAT 262). Procedure blanks of ~0.18 ng Nd and ~1.5 ng Sr are considered to have neglibible effect on the isotope measurements

Sample	Whole rock	Rb	Sr	Rb/Sr	$^{87}Rb/^{86}Sr$	$^{87}Sr/^{86}Sr_m$	$^{87}Sr/^{86}Sr_i$	ϵSr	Sm	Nd	Sm/Nd	$^{147}Sm/^{144}Nd$	$^{143}Nd/^{144}Nd_m$	$^{143}Nd/^{144}Nd_i$	ϵNd
SKX O1	Leached	0.56	507.8	0.0011	0.0032	0.70359	0.70358	–8.37	4.66	30.35	0.1536	0.0929	0.51248	0.51230	0.91
	Nonleached (ID)	73.53	739.1	0.0995	0.2877	0.70491	0.70368	–6.93	12.40	76.02	0.1631	0.0986	0.51249	0.51230	0.85
	Leached/ICP-MS	82	774	0.1059			0.70228	–26.74	13	68	0.1912			0.51225	0.05
SKX 14	Leached	0.98	702.4	0.0014	0.0040	0.70346	0.70344	–10.28	5.89	36.24	0.1625	0.0983	0.51248	0.51229	0.73
	Leached/ICP-MS	27	667	0.0405			0.70296	–17.12	10	55	0.1818			0.51227	0.29
SKX 34	Leached	1.20	78.1	0.0154	0.0445	0.70354	0.70335	–11.60	3.97	21.15	0.1876	0.1134	0.51259	0.51237	2.24
	Leached/ICP-MS	52	1251	0.0416			0.70303	–16.19	11	60	0.1833			0.51237	2.35
SKX 37B	Leached	0.25	1,073.1	0.0002	0.0007	0.70320	0.70320	–13.71	4.05	20.77	0.1948	0.1178	0.51256	0.51233	1.54
	Leached/ICP-MS	49	1,196	0.0410			0.70270	–20.85	14	67	0.2090			0.51231	1.22
SKX 49	Leached	14.93	898.0	0.0166	0.0481	0.70386	0.70365	–7.30	2.89	14.94	0.1936	0.1170	0.51255	0.51232	1.25
	Nonleached (ID)[a]	69.00	571.0	0.1208	0.3494	0.70483	0.70334	–11.76	8.20	42.40	0.1934	0.1169	0.51255	0.51232	1.28
	Leached/ICP-MS	57	846	0.0674			0.70303	–16.19	9	41	0.2098			0.51230	0.88
SKX 55	Leached	5.71	1,085.2	0.0053	0.0152	0.70370	0.70364	–7.54	3.81	16.48	0.2312	0.1398	0.51268	0.51240	2.96
	Nonleached (ID)[a]	34.30	940.0	0.0365	0.1056	0.70376	0.70331	–12.19	10.30	59.90	0.1720	0.1040	0.51263	0.51243	3.42
	Leached/ICP-MS	22	816	0.0270			0.70337	–11.34	10	51	0.1961			0.51245	3.78
SKX 70	Leached	5.50	1,937.4	0.0028	0.0082	0.70341	0.70338	–11.18	7.89	29.66	0.2660	0.1608	0.51251	0.51219	–1.13
	Leached/ICP-MS	61	1,739	0.0351			0.70298	–16.83	11	59	0.1864			0.51229	0.72[c]
Sample	Pyroxene type	Rb	Sr	Rb/Sr	$^{87}Rb/^{86}Sr$	$^{87}Sr/^{86}Sr_m$	$^{87}Sr/^{86}Sr_i$	ϵSr	Sm	Nd	Sm/Nd	$^{147}Sm/^{144}Nd$	$^{143}Nd/^{144}Nd_m$	$^{143}Nd/^{144}Nd_i$	ϵNd
SKX 01	Green (PhenDi)	0.12	158.7	0.0008	0.0022	0.70344	0.70343	–10.50	2.82	13.03	0.2166	0.1309	0.51255	0.51230	0.87
SKX 14	Green (PhenDi)	0.37	84.2	0.0044	0.0128	0.70336	0.70330	–12.30	1.17	5.96	0.1960	0.1185	0.51260	0.51236	2.20
SKX 34	Brown (Ti-augite)	0.11	364.6	0.0003	0.0008	0.70343	0.70343	–10.52	12.75	63.13	0.2019	0.1221	0.51257	0.51233	1.56
SKX 37B	MgDi	0.07	91.7	0.0007	0.0021	0.70328	0.70327	–12.78	1.16	4.76	0.2438	0.1474	0.51268	0.51239	2.73
SKX 37B	Green (PhenDi)	0.13	106.4	0.0012	0.0036	0.70336	0.70334	–11.74	n.d.	6.13	[b]		0.51266	0.51240	2.93
SKX 37B	Brown (Ti-augite)	0.05	113.6	0.0005	0.0013	0.70339	0.70339	–11.09	3.15	13.44	0.2344	0.1417	0.51264	0.51236	2.15
SKX 49	Brown (Ti-augite)	0.37	125.0	0.0029	0.0085	0.70366	0.70362	–7.76	5.42	20.94	0.2589	0.1565	0.51265	0.51234	1.77
SKX 55	Green (PhenDi)	0.70	76.6	0.0092	0.0266	0.70365	0.70354	–8.89	n.d.	5.21	[b]		0.51274	0.51242	3.26
SKX 63	Brown (Ti-augite)	2.29	71.7	0.0320	0.0925	0.70402	0.70362	–7.70	5.57	27.80	0.2004	0.1212	0.51257	0.51233	1.51
SKX 70	Brown (Ti-augite)	0.43	282.2	0.0015	0.0044	0.70323	0.70321	–13.63	12.43	58.94	0.2109	0.1275	0.51256	0.51231	1.04

[a] Data extracted from Anthony et al. (1989)
[b] Data from Dunworth et al. (in preparation)
[c] Used in Fig. 7

the Cr-diopsides nor the MgDi compositions contain significant amounts of the jadeite component, whereas TiO_2 contents of ~0.6 wt% are common, and thus higher than expected for mantle lherzolites. Jadeite-poor, Ti-rich Cr-diopsides appear to be uncommon in mantle material exhumed in alkaline and kimberlitic magmas.

Jadeite-poor MgDi compositions reported in mantle xenoliths in the literature include diopside found in a garnet pyroxenite vein from Pipe 200, Lesotho (PH 210, Carswell et al. 1979), a spinel websterite xenolith from the Hyblean Plateau, Sicily (Nimis and Vannucci 1995), a spinel garnet lherzolite xenolith in alnöite from Malaita, Solomon Islands (PH 4069, Nixon and Neal 1987), a discreet diopside nodule found in the type-locality Alnö alnöite (Kreston and Persson 1975), spinel lherzolite xenoliths from Nunivak, Alaska (Francis 1976, 1978), and deformed porphyroclastic–adcumulate wehrlitic xenoliths from the Adak and Kanga islands in the nearby Aleutian arc (Conrad and Kay 1983; Swanson et al. 1987). Ti contents remain relatively low in many of these examples (0.1–0.5 wt%).

A graphical comparison of the Skien pyroxene compositions with those from worldwide mantle xenoliths and cognate phenocryst growth in volcanic magmas is shown in Fig. 8, based on the multivariate statistical comparisons of Koloskov and Zharinov (1993). This shows clearly that the CrMgDi composiions are most unlikely to be cognate, and in fact bear closest resemblance to Kamchatka xenoliths. Figure 8 provides additional confirmation that, if the CrMgDi compositions are mantle xenocrysts, they are almost certainly not derived from a typical intraplate lherzolite. This may also be linked with the fact that xenocrystic olivine is so rarely found in the lavas, a feature hard to explain if the CrMgDi cores have been ripped up from an olivine-rich lherzolite by the host magmas – such xenocryst incorporation is rarely so phase-selective.

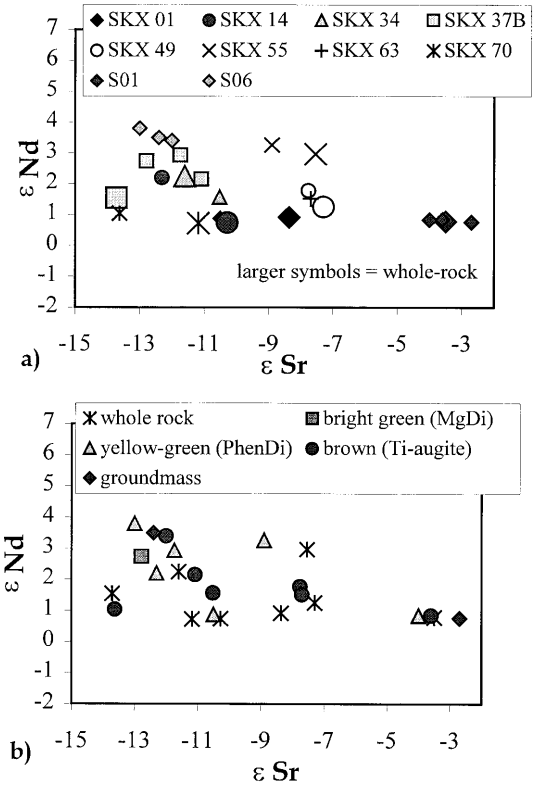

Fig. 7 ϵSr–ϵNd diagram at 300 Ma for leached pyroxene separates and whole-rock powders from Skien (cf. Table 4). **a** Pyroxene and whole-rock data plotted by sample number. **b** The same isotope data as in **a** plotted according to type of pyroxene, or whole-rock. Pyroxene separates were picked on the basis of colour, assuming a reasonable correlation between colour and composition as determined by microprobe analyses from the same samples

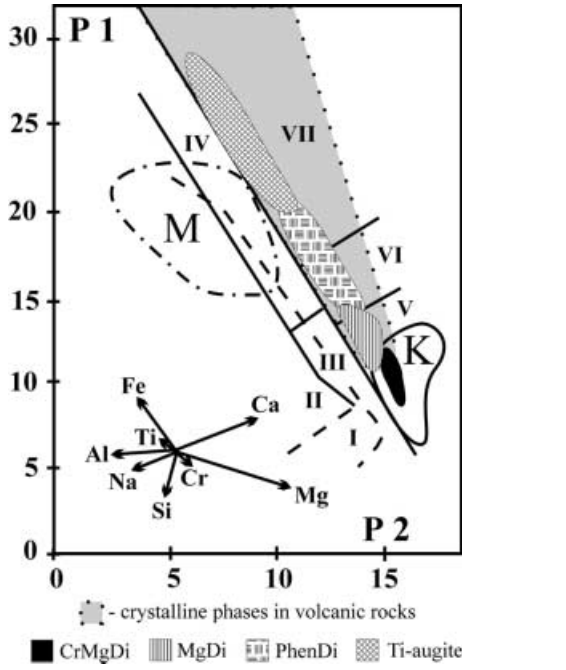

Fig. 8 Statistical multivariate plot of pyroxene compositions from Koloskov and Zharinov (1993). $P1 = -0.02SiO_2 + 0.09TiO_2 + 0.64Al_2O_3 + 0.59Cr_2O_3 + 1.35FeO + 9.65MnO - 0.5MgO + 0.29CaO - 2.26Na_2O + 8.0$; $P2 = -0.93TiO_2 + 0.07Al_2O_3 + 1.23Cr_2O_3 - 0.46FeO + 1.74MnO + 0.36MgO + 0.10CaO - 1.66Na_2O + 8.0$. *Areas I-VII* represent mantle xenolith compositions from particular tectonic settings. *I* Periodotites in kimberlites; *II* Eclogites in kimberlites; *III* Spinel lherzolites (continental alkali basalts); *IV* Spinel pyroxenites (continental alkali basalts); *V* Island arc peridotites; *VI* Island arc pyroxenites; *VII* Plagioclase-bearing xenoliths. Fields for crystalline pyroxenes (*grey shaded area*) and megacrysts (*M*) in volcanic rocks are also shown, along with the compositions of alpine-like ultrabasic rocks from Kamchatka (*K*). Additional data from the Skien CrMgDi and MgDi compositions (*black area*) are from the present study. Whereas many of the MgDi compositions overlap with the grey shaded area, the CrMgDi compositions do not

Partially melted and/or re-equilibrated mantle xenocrysts

A possible explanation for the low jadeite content of the CrMgDi compositions is that they are lherzolitic mantle xenocrysts which have undergone dissolution, either during magma ascent to the surface or prior to inclusion within the host magma. Fractional melting normally depletes the original pyroxene composition in Na and Al, enriches it in Ti, and leaves Cr and Mg contents virtually unchanged while creating a variety of melting textures in the process (Shaw and Edgar 1997). Similar chemical and textural effects are also seen in a partially melted clinopyroxene in an olivine-clinopyroxene xenolith from the Rhinegraben (Dunworth 1991). Equilibrium melting increases the Mg and Cr contents and Cr/(Cr + Al) ratios in the residual pyroxene, while decreasing the Na/(Na + Ca) ratio (Mysen and Kushiro 1977). Thus, it is possible that the CrMgDi cores could represent lherzolitic mantle xenocrysts which have undergone fractional melting.

There appears to be no means of creating the MgDi compositions as a residue from the CrMgDi cores via partial melting. However, MgDi compositions have been produced experimentally by disequilibrium melting of orthopyroxene in basanitic magmas at a variety of pressures (Shaw et al. 1998; Shaw 1999), although it is uncertain whether this could provide the quantity and range of MgDi compositions and textures seen in the Skien lavas, given the fact that these experiments only produced grains a few 100 μm in diameter.

Early cognate phenocrysts

Given the general lack of olivine in the Skien lavas, we cannot exclude the possibility that the CrMgDi and/or the MgDi compositions represent the earliest liquidus phase in these lavas. Similar low-jadeite compositions, described as cognate, have been found in an alkali basalt from Loihi Volcano, Hawaii (Garcia et al. 1995), ultramafic volcanics from Kamchatka (Kamenetsky et al. 1995), and shoshonitic lavas from Stromboli (Francalanci 1989). The similarity between the calculated trace-element composition of the early cognate pyroxenes and the MgDi compositions, combined with the formation of euhedral, glomeroporphyritic MgDi pyroxenes in

sample SKX 07, suggests that the MgDi compositions may indeed be representative of early cognate growth. If the MgDi compositions are indeed cognate, then their highest Cr contents may be explained by using a higher D_{Cr} for pyroxene/melt (e.g., Duke 1976; Dostal et al. 1983; Francalanci 1989) than the value of 4 obtained at 30 kbar by Hart and Dunn (1993). The CrMgDi compositions appear to be too depleted in trace elements to be cognate, and Fig. 8 confirms that they fall outside the field of known compositions from volcanic lavas (Koloskov and Zharinov 1993), suggesting that a xenocrystic origin may be more appropriate for these compositions.

Geothermobarometry

An inherent problem in attempting PT estimates of pyroxene formation in the Skien lavas is the lack of other phenocryst phases (e.g., olivine), which thus restricts the number and type of geothermometers and barometers available for use. As shown above, the Putirka et al. (1996) geothermobarometer gives ~12 kbar and ~1,250 °C for the MgDi pyroxenes from sample SKX 14, whereas the Soesoo (1997) geothermobarometer gives < 3 kbar and 1,115–1,160 °C for the Ti-augite compositions. The CrMgDi and MgDi compositions fall outside the calibrated field of Soesoo (1997; see Fig. 3f). It should be noted that clinopyroxene crystallized experimentally as a result of orthopyroxene dissolution within a basanitic magma under dry disequilibrium conditions at 1 GPa (Shaw 1999) would plot almost exactly on top of the MgDi and CrMgDi compositions in Fig. 3f (data not shown), supporting the Putirka et al. (1996) PT estimates for the MgDi crystallization conditions, and confirming that the geothermobarometer of Soesoo (1997) is not correctly calibrated for these compositions.

The MgDi and Ti-augite PT estimate place the earliest, cognate pyroxene crystallization at the MOHO, and the last stage of crystallization at upper crustal levels. This appears to be geologically reasonable, and matches geophysical evidence for MOHO-depth and deep-crustal cumulates (Neumann 1994, and references therein).

Similar MgDi pyroxene cores are also found in the B1 Vestfold lavas, northeast of Skien (Fig. 1; Dunworth, unpublished data). The more fractionated rhomb-porphyry latite lavas which lie above the Vestfold B1 basalts were estimated to have formed as the result of fractionation processes at 6.5–10 kbar (Neumann 1994). This suggests that the earlier, more mafic lavas, whose groundmass compositions are trachyandesitic, should also have begun to fractionate at this depth, a fact supported by the MgDi ~12 kbar crystallization estimate given above.

Overall, we favour a xenocrystic source for the Cr-diopside cores, although this source is unlikely to be lherzolitic in composition. If cognate, their extremely depleted compositions would necessitate crystallization from an unusually depleted mantle melt, the like of which is not seen in the trace-element-rich, mafic Skien lavas, and thus we provisionally rule out a cognate origin. Textural and chemical evidence suggests that the diopside phenocryst and Ti-augite pyroxenes crystallized directly out of the Skien lavas, although their nonequilibrated isotopic signatures suggest that there has been some magma mixing and/or crustal contamination since the crystallization of the diopside compositions. This leaves the moderately depleted MgDi compositions which show the greatest textural variations – glomeroporphyritic clusters of twinned subhedral crystals, strained anhedral crystals, and resorbed and partially melted cores. We favour a cognate origin related to the same magmatic event that gave rise to the Skien lavas, but perhaps related to early cumulates formed near the MOHO or within the lower crust (Olsen et al. 1987) and which were subsequently incorporated into the lavas which reached the surface. Work in progress on MgDi- and CrMgDi-hosted melt inclusions should help to resolve this issue in the near future (Kirstein et al., in preparation), and enable us to derive an overall model consistent with all the petrological, thermobarometric, and geophysical data available for this part of the Oslo Rift.

Isotopic disequilibrium – real or artefact?

Table 4 lists Sr-Nd isotope data for individual samples. At first glance, this provides evidence of intrasample isotopic disequilibrium (see above). However, it is also probable that some of the variations are secondary in origin. Trace-element whole-rock analyses from the basalts throughout the Skien sequence show that Rb and U in particular have been subjected to open-system behaviour since crystallization (Dunworth, unpublished data), due to postmagmatic (hydrothermal) alteration. It is for this reason that both the whole-rock sample powders and pyroxenes were heavily leached in hot HCl prior to analysis, in order to remove the majority of the low-temperature alteration and to identify the original isotopic signatures of the rocks. The presence of crustal (secondary) Sr is evident when the Sr isotope ratios of leached and nonleached powders are compared, a discrepancy that cannot be due only to the radioactive decay of primary magmatic Rb over the last 300 Ma. The leaching process, however, tends to remove much of the original Rb from the whole-rock powders, hence the leached Rb/Sr concentrations measured by isotope dilution are artificially low, yielding back-corrected initial $^{87}Sr/^{86}Sr$ ratios which are too high (Table 4).

Some researchers have preferred to leach whole-rock powders to determine the unaltered, measured isotopic values, while using Rb-Sr and Sm-Nd concentration data from nonleached powders to back-correct the leached isotopic values to their "initial" values. The effects of this procedure on the Skien basalts is seen in Table 4 in the "leached/ICP-MS" lines, where the leached

measured $^{87}Sr/^{86}Sr$ and $^{143}Nd/^{144}Nd$ signatures have been back-corrected to initial values using ICP-MS concentration data on the same nonleached powders. It can be seen that the resulting Sr epsilon values are exceptionally low, presumably due to the fact that some of the Rb present in the nonleached powders is of secondary origin. Overall, these results imply that bulk-rock isotope data, obtained from leached or nonleached material from the Skien lavas, should be treated with caution.

Since clinopyroxenes tend to have naturally low Rb/Sr values, little correction is needed to determine their initial $^{87}Sr/^{86}Sr$ ratios (e.g., Rosenbaum et al. 1996), and thus acid-leaching should preserve the primary isotopic signature of the clinopyroxene while removing secondary alteration (but not genuine pyroxene overgrowth). Thus, assuming isotopic equilibrium at the time of crystallization, each generation of pyroxene should record the isotopic composition of the magma from which it formed. If magma mixing or crustal contamination of the source magma occurred continuously during pyroxene growth, the compositions we observe would represent an average of these processes. The different generations of pyroxene thus preserve snapshots of magmatic evolution within individual flows which would be missed if only bulk-rock samples were analyzed.

Isotopic signatures

Many of the pyroxene trace-element variations discussed above are reflected in the Sr-Nd isotope data. The "green" pyroxenes in Fig. 7b represent PhenDi compositions sensu stricto (see Fig. 3) but, given the limitations of mineral picking on the basis of colour, they may also contain some MgDi component. These phenocryst compositions are thought to represent the geochemical conditions prevailing in crustal and/or subcrustal magma chambers and, on average, they have slightly higher ϵNd and lower ϵSr values than the later generation of Ti-augite growth. The particular similarity between the Ti-augite and whole-rock compositions (particularly in ϵNd space) documented for many of the samples suggests that the compositions of the Ti-augites represent the conditions prevailing during late-stage magma crystallization. The changes in isotopic composition between the early- and late-stage pyroxenes provide good evidence for magma mixing and/or crustal contamination during magma evolution. More analyses (including those for Pb isotopic composition) are currently in progress to test these assumptions. Our new isotope data for the Skien samples agree well with those obtained in previous studies (Neumann et al. 1988; Anthony et al. 1989), and confirm that the Skien lavas contain contributions derived from at least one mantle source with low epsilon Sr and Nd values that was not involved in the production of the rest of the Oslo Rift lavas (Dunworth et al. 1999).

Magma mixing

Evidence for crustal-level magma mixing in the Skien basalts can be demonstrated using both the geochemistry and petrography of the pyroxenes. There are clear increases in $^{87}Sr/^{86}Sr_i$ from core to rim compositions, indicating mixing of a primitive, isotopically depleted magma with either a more enriched magma or crustal contaminants (Table 4, Fig. 7). Figure 5 also provides detailed evidence of magma mixing and the processes associated with it. The crystal shown in Fig. 5a contains a small MgDi core originally overgrown, presumably at low pressures (Fig. 3f), by concentrically and sector-zoned Ti-augite. The crystal was subsequently subjected to a sector-selective dissolution event within the magma chamber. Data on the chemical compositions of sector-zoned "hourglass" clinopyroxenes (Ferguson 1973; Downes 1974) imply that the [111] sectors (with central external apices) would have been more Si-Mg-Ti-rich than the [ab0] sectors which have been selectively melted in this sample, thus implying that the [111] sectors had higher solidus temperatures, or were closer to equilibrium with the host magma. The [ab0] sectors now contain a honeycomb network of small diopside cores (containing <0.4 wt% Cr_2O_3) which are overgrown with thin ~Cr-free Ti-augite rims, similar in composition to the Ti-augite found throughout the [111] sectors (Fig. 5b, c). It is believed that this melting and recrystallization process was due to an influx of hot magma into the magma chamber. When the newly replenished magma in the magma chamber cooled sufficiently, it precipitated a thin fresh rim of high-Cr (up to 1.0 wt% Cr_2O_3) Mg-poor diopside (Fig. 5), followed by an outer rim of ~Cr-free Ti-augite. Given the extreme compatibility of Mg and Cr in clinopyroxene, it is inconceivable that the late-stage high-Cr Mg-poor rim (shown white in Fig. 5a, b) could have been precipitated simply by a sudden rapid cooling event within the host magma, given that the Cr-rich rim lies outside (and has thus overgrown) an earlier phase of Ti-augite growth. The most logical reason for the observed textures and compositions lies in the magma-mixing process described above. A similar argument can be put forward to explain the thin (white) diopside overgrowth in Fig. 2a that lies between two generations of Ti-augite precipitation.

Further work, involving the collection of a larger whole-rock and mineral-separate isotope and trace-element dataset currently underway, will aim to further characterize and begin to quantify the nature of these mixing and contamination processes.

Magma-chamber processes

We propose the following model of magma evolution to describe the processes operating at Skien about 300 Ma ago. The parental magmas were derived from a sub-lithospheric source which was enriched in trace elements, and had low but potentially variable ϵSr and ϵNd values.

The contribution of a mantle component similar to the modern-day HIMU reservoir, as suggested by Anthony et al. (1989), is still probable but its source location cannot be confirmed at this time. Partial melting of the sublithospheric source ultimately produced the first, and most extensive B1-basalt sequence within the Oslo Rift, at Skien (Neumann et al. 1992). Between the initiation of sublithospheric melting and the eruption of the magmas at the surface, the magmas assimilated material from the mantle lithosphere, and fractionated within crustal or subcrustal magma chambers. It is assumed that any mantle material assimilated into the lavas was poor in olivine, and perhaps of garnet-pyroxenite composition (see above). Any garnet and orthopyroxene would dissolve in an alkali basaltic or basanitic melt (Eggler 1974; Brearly and Scarfe 1986; Shaw et al. 1998; Shaw 1999).

We propose that there were periods of melt influx from the mantle to the crustal plumbing system, perhaps incorporating (CrMgDi) or crystallizing (MgDi and/or PhenDi) a fresh set of diopsidic pyroxenes along the way, some of which made their way relatively rapidly towards the surface, and some of which underwent dissolution and Ti-augite overgrowth processes within the magma chamber. Towards the top of the main Skien sequence, the lavas generally become more fractionated and pyroxene-plagioclase-phyric, indicating longer periods between refilling of the magma chamber, and prolonged periods of magma-chamber fractionation.

Concluding remarks

1. The Skien lavas contain multiple generations of clinopyroxene, ranging in composition from Mg-rich Cr-diopsides to Ti-augite.

2. The early generations of pyroxene have been derived from a variety of sources, and are not in geochemical or isotopic equilibrium with each other or with their host melts.

3. Low-jadeite, Cr-diopside cores found in five samples, which exhibit a depleted trace-element signature, are believed to represent lithospheric mantle xenocrysts.

4. MgDi compositions are believed to represent very early cognate growth, or cumulate material preserved at deep-crustal levels which has been incorporated into later lavas.

5. The MgDi and PhenDi pyroxenes preserve an isotopic signature consistent with derivation from a mantle reservoir with an isotopic signature of approximately ϵSr–13 and ϵNd + 3.

6. Textural characteristics, isotopic and trace-element signatures show that the Ti-augite compositions were the last to crystallize, and that they crystallized in equilibrium with their host melts.

7. Calculated partition coefficients, based on pyroxene and whole-rock data, show that the middle and heavy HREE, along with Zr, Hf, and Y, are compatible in Ti-augite at low pressures. Nb, Sr, the LREE, and the LILE are incompatible under these conditions.

8. Irrefutable evidence of magma mixing and possible crustal contamination have been documented by the geochemical and textural characteristics of different generations of pyroxene growth.

The intrasample isotopic disequilibrium first documented by Anthony et al. (1989) has been confirmed and extended by this study. We have quantified and described the different pyroxene types extant in the formation, and have correlated type with major- and trace-element as well as Sr-Nd isotopic data. Work in progress will extend this disequilibrium dataset across Skien and the more extensive Vestfold and Jeloya pyroxene-phyric lavas further north, and enable more extensive constraints to be placed on the various mantle sources of these lavas and their differentiation histories.

Acknowledgements The authors would like to thank Jon Blundy and Cliff Shaw for thought-provoking reviews, Toril Enger for patient assistance in the chemistry lab, Tom Andersen and Bjørn Sundvoll for taming the mass spectrometers, Håkon Austrheim and Muriel Erambert for troubleshooting on the microprobe, Linda Kirstein for cheerful assistance and comments on earlier drafts of this manuscript, and John Craven for his technical wizardry with the ion microprobe. Partial support for the ion microprobe time came via NERC grant IMP/123/1097 to JMR. This work has been carried out as part of an EU-funded TMR network – Permo-Carboniferous Rifting in Europe (project reference ERB-FMRXCT960093).

References

Anthony EY, Segalstad TV, Neumann E-R (1989) An unusual mantle source region for nephelinites from the Oslo Rift, Norway. Geochim Cosmochim Acta 53:1067–1076

Blundy JD, Robinson JC, Wood BJ (1998) Heavy REE are compatible in clinopyroxene on the spinel lherzolite solidus. Earth Planet Sci Lett 160:493–504

Brearly M, Scarfe CM (1986) Dissolution rates of upper mantle minerals in an alkali basalt melt at high pressure: an experimental study and implications for ultramafic xenolith survival. J Petrol 27:1157–1182

Carswell DA, Clarke DB, Mitchell RH (1979) The petrology and geochemistry of ultramafic nodules from Pipe 200, Northern Lesotho. In: Boyd FR, Meyer HOA (eds) The mantle sample: inclusions in kimberlites and other volcanics. Proc 2nd Int Kimberlite Conference, Vol 2. AGU, Washington, DC, pp 127–144

Conrad WK, Kay RW (1983) Ultramafic and mafic inclusions from Adak Island: crystallization history, and implications for the nature of primary magmas and crustal evolution in the Aleutian Arc. J Petrol 25:88–125

Dostal J, Dupuy C, Carron JP, Le Guen de Kerneizon M, Maury RC (1983) Partition coefficients of trace elements: application to volcanic rocks of St. Vincent, West Indies. Geochim Cosmochim Acta 47:525–533

Downes MJ (1974) Sector and oscillatory zoning in calcic augites from M. Etna, Sicily. Contrib Mineral Petrol 47:187–196

Duda A, Schmincke H-U (1985) Polybaric differentiation of alkali basaltic magmas: evidence from green-core clinopyroxenes (Eifel, FRG). Contrib Mineral Petrol 91:340–353

Duke JM (1976) Distribution of the period four transition elements among olivine, calcic clinopyroxene and mafic silicate liquid: experimental results. J Petrol 17:499–521

Dunworth EA (1991) A geochemical and petrogenic study of olivine melilitites from the Tertiary-Quaternary Volcanic Province of Southern Germany. MSc Thesis, University of Leeds
Dunworth EA, Bell K (2001) The Turiy Massif, Kola Peninsula, Russia: Isotopic and geochemical evidence for multi-source evolution. J Petrol (in press)
Dunworth EA, Wilson M (1998) Olivine melilitites of the SW German Tertiary Volcanic Province: mineralogy and petrogenesis. J Petrol 39:1805–1836
Dunworth EA, Neumann E-R, Rosenbaum JM (1999) Mantle reservoirs, xenocrysts and magmatic disequilibrium in the Skien basalts, Oslo Rift. Abstr Vol Eur Union Geosci Conf No 10, Strasbourg, 28 March–1 April 1999, pp 291
Eggler DH (1974) Effects of CO_2 on the melting of peridotite. Carnegie Inst Wash Yearb 73:215–224
Ferguson AK (1973) On hour-glass zoning in clinopyroxene. Mineral Mag 39:321–325
Francalanci L (1989) Trace element partition coefficients for minerals in shoshonitic and calc-alkaline rocks from Stromboli Island (Aeolian Arc). Neues Jahrb Mineral Abh 160:229–247
Francis DM (1976) The origin of amphibole in lherzolite xenoliths from Nunivak Island, Alaska. J Petrol 17:357–378
Francis DM (1978) The implications of the compositional dependence of texture in spinel lherzolite xenoliths. J Geol 86:473–485
Frey FA, Prinz M (1978) Ultramafic inclusions from San Carlos, Arizona: Petrologic and geochemical data bearing on their petrogenesis. Earth Planet Sci Lett 38:129–176
Garcia MO, Foss DJP, West HB, Mahoney JJ (1995) Geochemical and isotopic evolution of Loihi volcano, Hawaii. J Petrol 36:1647–1674
Griffin WL (1973) Lherzolite nodules from the Fen alkaline complex, Norway. Contrib Mineral Petrol 38:135–146
Hart SR, Dunn T (1993) Experimental cpx/melt partitioning of 24 trace elements. Contrib Mineral Petrol 113:1–8
Heeremans M, Larsen BT, Stel H (1996) Paleostress reconstruction from kinematic indicators in the Oslo Graben, southern Norway: new constraints on the mode of rifting. Tectonophysics 266:55–79
Hinton RW, Harte B, Witteickschen G (1995) Ion probe measurements of National-Institute-of-Standards-and-Technology standard reference material SRM-610 glass, trace-elements. Analyst 120:1315–1319
Kamenetsky VS, Sobolev AV, Joron J-L, Semet P (1995) Petrology and geochemistry of Cretaceous ultramafic volcanics from Eastern Kamchatka. J Petrol 36:637–662
Koloskov AV, Zharinov SE (1993) Multivariate statistical analysis of clinopyroxene compositions from mafic and ultramafic xenoliths in volcanic rocks. J Petrol 34:173–185
Kresten P, Persson L (1975) Discrete diopside in alnöite from Alnö Island. Lithos 8:187–192
Mearns E (1986) Sm-Nd ages for Norwegian garnet peridotites. Lithos 19:269–278
McDonough WF, Sun S-S (1995) The composition of the Earth. Chem Geol 120:223–253
Mysen BO, Kushiro I (1977) Compositional variations of coexisting phases with degree of melting of peridotite in the upper mantle. Am Mineral 62:843–865
Neumann E-R (1986) Mass estimates of cumulates and residues after anatexis in the Oslo Graben. J Geophys Res 91(B11):11629–11640
Neumann E-R (1994) The Oslo Rift: P-T relations and lithospheric structure. Tectonophysics 240:159–172
Neumann E-R, Tilton GR, Tuen E (1988) Sr, Nd and Pb isotope geochemistry of the Oslo rift igneous province, southeast Norway. Geochim Cosmochim Acta 52:1997–2007
Neumann E-R, Sundvoll B, Overli PE (1990) A mildly depleted upper mantle beneath southeast Norway: evidence from basalts in the Permo-Carboniferous Oslo Rift. Tectonophysics 178:89–107
Neumann E-R, Olsen KH, Baldridge WS, Sundvoll B (1992) The Oslo Rift: a review. Tectonophysics 208:1–18
Neumann E-R, Wulff-Pedersen E, Simonsen SL, Pearson NJ, Martí J, Mitjavila J (1999) Evidence for fractional crystallization of periodically refilled magma chambers in Tenerife, Canary Islands. J Petrol 40:1089–1123
Nimis P, Vannucci R (1995) An ion microprobe study of clinopyroxenes in websteritic and megacrystic xenoliths from Hyblean Plateau (SE Sicily, Italy): constraints on HFSE/REE/Sr fractionation at mantle depth. Chem Geol 124:185–197
Nixon P (ed) (1987) Mantle xenoliths. Wiley, New York
Nixon PH, Neal CR (1987) Ontong Java Plateau: deep-seated xenoliths from thick oceanic lithosphere. In: Nixon P (ed) Mantle xenoliths. Wiley & Sons, New York, pp 335–345
Olsen KH, Baldridge WS, Larsen BT, Neumann ER, Ramberg IB (1987) A lithospheric transect across the Oslo palaeorift. EOS 68:1480
Pearce NJG, Perkins WT, Westgate JA, Gorton MP, Jackson SE, Neal CR, Chenery SP (1997) A compilation of new and published major and trace element data for NIST SRM 610 and NIST SRM 612 glass reference materials. Geostds Newslett 21:115–144
Putirka K, Johnson M, Kinzler R, Longhi J, Walker D (1996) Thermobarometry of mafic igneous rocks based on clinopyroxene-liquid equilibria, 0–30 kbar. Contrib Mineral Petrol 123:92–108
Ramberg IB (1976) Gravity interpretation of the Oslo Graben and associated igneous rocks. Norges Geol Unders 325:1–194
Ramberg IB, Larsen BT (1978) Tectonomagmatic evolution. Norges Geol Unders 337:55–73
Ro HE, Stuevold LM, Faleide JI, Myhre AM (1990) Skagerrak Graben – the offshore continuation of the Oslo Graben. Tectonophysics 178:1–10
Rocholl A, Ludwig T, Altherr R, Meyer HP, Brey G, Velz S, Seck HA, Bulatov V (1996) Experimental partitioning of trace elements between clinopyroxene, garnet and basanitic melts studied by ion microprobe. J Conf Abs 1:555
Roeder PL, Emslie RF (1970) Olivine-liquid equilibrium. Contrib Mineral Petrol 29:275–289
Rosenbaum JM, Zindler A, Rubenstone JL (1996) Mantle fluids: Evidence from fluid inclusions. Geochim Cosmochim Acta 60:3229–3252
Schou-Jensen E, Neumann E-R (1988) Volcanic rocks on Jeloya, central Oslofjord: The mafic lavas. Norges Geol Tidsskr 68:289–308
Segalstad TV (1979) Petrology of the Skien basaltic rocks, southwestern Oslo Region, Norway. Lithos 12:221–239
Shaw CSJ (1999) Dissolution of orthopyroxene in basanitic magma between 0.4 and 2 GPs: further implications for the origin of Si-rich alkaline glass inclusions in mantle xenoliths. Contrib Mineral Petrol 135:114–132
Shaw CSJ, Edgar AD (1997) Post-entrainment mineral-melt reactions in spinel peridotite xenoliths from inver, Donegal, Ireland. Geol Mag 134:771–779
Shaw CSJ, Thibault Y, Edgar AD, Lloyd FE (1998) Mechanisms of orthopyroxene dissolution in silica-undersaturated melts at 1 atmosphere and implications for the origin of silica-rich glass in mantle xenoliths. Contrib Mineral Petrol 132:354–370
Skulski T, Minarik W, Watson EB (1994) High-pressure experimental trace-element partitioning between clinopyroxene and basaltic melts. Chem Geol 117:127–147
Soesoo A (1997) A multivariate statistical analysis of clinopyroxene composition: empirical coordinates for the crystallisation PT-estimations. Geol Fören Stockholms Förhand 119:55–60
Sundvoll B, Larsen BT (1994) Architecture and early evolution of the Oslo Rift. Tectonophysics 240:173–189
Sundvoll B, Neumann E-R, Larsen BT, Tuen E (1990) Age relations among Oslo Rift magmatic rocks: implications for tectonic and magmatic modelling. Tectonophysics 178:67–87
Swanson SE, Kay SM, Brearly M, Scarfe CM (1987) Arc and back-arc xenoliths in Kurile-Kamchatka and western Alaska. In: Nixon PH (ed) Mantle xenoliths. Wiley, New York, pp 302–318